Ant-Inspired Control Strategies for Collective Transport by Dynamic Multi-Robot Teams with Temporary Leaders

by

Elikplim Gah

A Thesis Presented in Partial Fulfillment
of the Requirements for the Degree
Master of Science

Approved April 2020 by the
Graduate Supervisory Committee:

Spring Berman, Chair
Theodore Pavlic
Hamidreza Marvi

ARIZONA STATE UNIVERSITY

May 2020

ABSTRACT

In certain ant species, groups of ants work together to transport food and materials back to their nests. In some cases, the group exhibits a leader-follower behavior in which a single ant guides the entire group based on its knowledge of the destination. In some cases, the leader role is occupied temporarily by an ant, only to be replaced when an ant with new information arrives. This kind of behavior can be very useful in uncertain environments where robot teams work together to transport a heavy or bulky payload. The purpose of this research was to study ways to implement this behavior on robot teams.

In this work, I combined existing dynamical models of collective transport in ants to create a stochastic model that describes these behaviors and can be used to control multi-robot systems to perform collective transport. In this model, each agent transitions stochastically between roles based on the force that it senses the other agents are applying to the load. The agent's motion is governed by a proportional controller that updates its applied force based on the load velocity. I developed agent-based simulations of this model in NetLogo and explored leader-follower scenarios in which agents receive information about the transport destination by a newly informed agent (leader) joining the team. From these simulations, I derived the mean allocations of agents between "puller" and "lifter" roles and the mean forces applied by the agents throughout the motion.

From the simulation results obtained, we show that the mean ratio of lifter to puller populations is approximately 1:1. We also show that agents using the role update procedure based on forces are required to exert less force than agents that select their role based on their position on the load, although both strategies achieve similar transport speeds.

ACKNOWLEGMENTS

I'd like to acknowledge my professor and thesis advisor, Spring M. Berman, Ph.D., for all her help throughout this project. I am extremely grateful to have had the opportunity to work with her. The insights and guidance she provided were really the only reason why I was able to make any progress at all.

I would also like to thank all my colleagues in ACS Lab, especially Zahi Kakish and Hamed Farivarnejad for all their support throughout this period. I am grateful for the critiques of my work, and for the explanations of concepts that I had difficulty comprehending on my own.

I would also like to thank Prof. Hamidreza Marvi for his wonderful tutelage during what was my first actual class in robotics. His approach to teaching allowed me to develop a real interest in the field and I will miss his classes.

I would also like to thank Prof. Eric Knott of the W.P. Carey School of Business. His help and guidance allowed me to pull through a time of depression and back onto my feet. He allowed me to get on with my work and I am truly grateful for his help.

I am also grateful to the MasterCard Foundation for making it possible for me to pursue graduate studies.

TABLE OF CONTENTS

Page

CHAPTER Page

LIST OF TABLES

Table Page

LIST OF FIGURES

Figure Page

Figure Page

Figure Page

Figure Page

Figure Page

NOMENCLATURE

v_{cm}	→	Velocity of center of mass of load
ω	→	Angular velocity of load
f_0/τ_0	→	Force / Torque exerted by single puller
$f_{kin}/\ \tau_{kin}$	→	Force/Torque due to kinetic friction on the load
$\gamma\ /\gamma_{rot}$	→	Load response coefficient for force/ torque
∂v_{cm}	→	v_{cm} as load is at rest when pullers begin to pull
f_{tot}/f_{cm}	→	Total force exerted on load at its center of mass
θ_i	→	Point of attachment of puller *i* on circumference of load
ϕ_i	→	Angle between head of puller *i* and point of attachment
$n_p(\theta_i\ , \phi_i)$	→	$\begin{cases} 1 & ,if\ site\ is\ occupied\ by\ puller \\ 0 & ,if\ site\ is\ empty \end{cases}$
K_{off}^1	→	Detachment rate from stationary load
K_{off}^2	→	Detachment rate from moving load
K_{detach}	→	Overall Detachment rate
K_{on}	→	Attachment rate
f_{loc}	→	Force sensed by puller at attachment point
P_p	→	Probability of becoming a puller
P_l	→	Probability of becoming a lifter
p_i	→	Polarization vector
K_c	→	Rate at which ants change roles when attached to static load & rate at which ants reorient themselves with velocity of the load

INTRODUCTION

Collective transport by multi-robot teams has been a topic of much study over the past two decades due to the potential applications in such a wide variety of scenarios. Having teams of robots perform tasks eliminates the need for high complexity in design and control that is required to enable only one robot perform that same task. It allows for more dynamic teams that can be either homogeneous (all team members having the same capabilities) or heterogeneous (different team members having different capabilities). With either implementation, what is developed is a system that has some relative latitude to perform an array of tasks.

Much progress has been made in developing control strategies for single-robot behaviors. Path planning, trajectory control and even navigation are problems that have been solved for many types of environments using varying strategies. Further work is being devoted to the control of multi-robot team dynamics, especially using advances in decision-making algorithms that the team members can use. For many of these problems, solutions can be readily found in nature. Studies of organisms that exhibit collective behaviors, especially social insects, reveal a "swarm intelligence" that seems to govern the actions of the members of the swarm (Bonabeau, et al., 1999). It then becomes a question of understanding the behaviors of individual organisms and applying these strategies to robot teams to achieve similar global behaviors, all the while taking into consideration the capabilities of the robot teams (Brambilla, et al., 2013).

Over the past couple of decades, considerable effort has been invested in developing multi-robot systems for various use cases, including the following:

1. *Manufacturing*: This has been one of the most natural partnerships of technology and industry we have seen. Automotive manufacturing companies make use of industrial robots in their product lines, and manufacturers of products such as electronics, medical equipment and food processing equipment are employing robot teams to achieve various tasks. An example is the SWARM robot project by Rolls Royce, which will measure around 10mm in diameter and will be used to inspect the insides of engines.
2. *Medicine*: Medical procedures that have been the sole domain of human professionals are now being assisted by robots. The I-SWARM project (Seyfried, et al., 2005) sought to develop micro-robots with a planned size of $2\times2\times1mm^3$ capable of implementing swarm behavior to deliver medicines or inspect internal organs, reducing the need for invasive procedures. (Martel, et al., 2009) demonstrates the integration of bacteria with nanorobots or other micro-scale entities to use their molecular motors as a means of propulsion and describes their potential for applications in human blood vessels. Applications include targeting tumoral lesions for treatments.
3. *Construction*: The world's greatest builders may be termites, and we continue to search ways to mimic these organisms, as shown in the work on termite-inspired multi-robot construction in (Werfel, 2012).
4. *Space Exploration*: The Mars exploration rovers (Spirit, Opportunity and Curiosity) are the best examples of this use case. Without the ability to send humans on these exploratory expeditions, robots have been our most effective tool. The "Swarmie" is also another example of a robot designed for applications in space exploration

(Leucht, 2016). When complete, the robots will be capable of scanning for water-ice or other resources that can be turned into rocket fuel or breathable air.

5. *Home service automation*: Lots of homes today have an autonomous lawnmower or vacuum robot. Roombas and other cleaning robots have become a part of the everyday technological landscape, and their popularity and functionality keep on increasing.

Collective transport is one such problem that is readily solved by multiple species, especially in ants. Understanding how different ant species achieve this should enable the implementation of collective transport strategies across various robot platforms. Whilst there are certainly other species that could be investigated, ants are especially suitable for study due to their small size and relatively simple behaviors. The level of complexity in recreating the behavior of an individual is thus reduced significantly.

The work in this thesis is inspired by the research carried out in Dr. Spring Berman's lab on developing control policies for robotic swarms based on a study of the desert ant *Novomessor cockerelli*. The other major influence on this thesis is the work done by Dr. Ofer Feinerman's lab on collective transport by the *Paratrechina longicornis* species.

1.1 Literature Review

This section highlights the work done in swarm robotics with respect to collective transport and swarming behaviors. The focus is on studies that seek to model and emulate or replicate collective transport behaviors in ants. Typically, these studies address some combination of the following three problems:

1. Development of a dynamical model of the transporters and their load
2. Determining the composition of the transport team (e.g., the roles that robots assume during transport)
3. Design of decentralized robot control strategies for transport

In (Kube & Bonabeau, 2000), an ant-inspired control strategy that allows robots to reposition themselves on the load during a box-pushing task is investigated. (Rubenstein, et al., 2013) describes a physics-based model for the dynamics of a multi-robot collective transport process, breaking the problem down into two phases. The first phase involves the robots searching for and attaching to the load, and the second phase involves the robots applying forces to the load to achieve transport.

In their work on *N. cockerelli,* (Berman, et al., 2011) develop a hybrid dynamical model for group food retrieval by these ants based on experimental data. (Kumar, et al., 2013) build on this work to develop a Stochastic Hybrid System (SHS) model for collective transport by ants of the same species. This SHS model describes the time evolution of ant behaviors (resulting from stochastic switching of ants between roles), as well as the load position and population counts of ants in different roles.

Further work on these ant-inspired stochastic behaviors is presented in (Pavlic, et al., 2016), which allows robots to interact with each other and with the boundaries of multiple loads to achieve target robot populations around each type of load without requiring analytical expressions for the corresponding encounter rates. The work describes stochastic policies that allow robots to "*avoid collisions with each other, bind to boundaries of disk-shaped regions, and command bound robots to unbind*" (Pavlic, et al., 2016).

(Wilson, et al., 2014) describes control policies derived from the SHS model developed in (Kumar, et al., 2013) and also extends the work done in (Pavlic, et al., 2016). This work presents three methods for designing the control policies that "*mimic different microscopic and macroscopic properties of collective transport in ants.*"

(Pavlic, et al., 2014) also builds on this prior work and (Wilson, et al., 2014). In this extension of the work, they propose control policies that implement spontaneous ant detachment from the load as a catalytic process based on agent encounters. A reduced-order model is also proposed which can approximate the system dynamics of the swarm.

The Feinerman group has carried out studies on *P. longicornis*, whose behavior during collective transport allow them to incorporate information from temporary leaders. (Gelblum, et al., 2015) presents an Ising model of this behavior that describes the "*decision rules that balance individuality and compliance. Macroscopically, these rules poise the system at the transition between random walk and ballistic motion where the collective response to the steering of a single informed ant is maximized."*

1.2 Outline of Thesis

Chapter 2 details the mathematical equations and computations used to describe and model the macroscopic, or population-level, and microscopic, or individual-level, behaviors of a swarm as it performs collective transport.[1] Chapter 3 describes the agent controller design and implementation of the model in an agent-based simulation.

[1] Most of these equations are taken from the (Feinerman, et al., 2018) and (Pavlic, et al., 2014) papers.

Simulation results are provided and discussed in Chapter 4. Conclusions and possible directions for future work are given in Chapter 5.

1.3 Contributions of Thesis

Most ant-inspired collective transport models assign agent roles based on the location of the agent on the payload. One common scheme involves dividing the payload into two distinct regions (front and back) with respect to the direction of transport and assigning each agent's role based on which of the two regions the agent is attached to. While this scheme has been shown to successfully produce collective transport in simulation and experiments, collective transport behaviors observed in ants (at least, in *P. longicornis*) include switching of transporters between roles in response to the forces that they perceive are being exerted on the payload (Feinerman, et al., 2018).

This thesis combines the model of collective transport proposed in (Pavlic, et al., 2014) with the role change rules and role selection probabilities defined in the Ising model described in (Feinerman, et al., 2018). The result is a stochastic dynamical model of a robot-payload system that allows the agents to change roles throughout the transport task. Using agent-based simulations in NetLogo, an exploration is also made into the effect that transient leaders have on the group. It is shown that the agents achieve an equilibrium state where the number of agents pulling the load is approximately equal to the number of agents lifting the load. It is also shown that this equilibrium state is achieved irrespective of the points of attachment of agents on the load or the number of agents attached to the load. It is also shown that under the suggested role update procedure, the forces exerted by the members of the transport team are significantly lower than an implementation where the robots select roles based on their positions on the payload.

2 MATHEMATICAL MODEL

The load dynamics and rules for ant selection of pulling and lifting roles while attached to the load are based on the work done on the effects of transiently informed individuals on ant group behavior (Gelblum, et al., 2015).

The model for ant movement while searching for the load and the control policies for ant attachment to/detachment from the load are based primarily on the models in (Pavlic, et al., 2014), (Pavlic, et al., 2016) and (Wilson, et al., 2014).

A key for the symbols and variables used in the equations in this section can be found in the Nomenclature table (see beginning of document).

2.1 Load Dynamics

Here, we present a description of the dynamical model of the load. When an ant is attached to the load, it exerts a force on the load in a bid to transport it to some location. The ant attaches itself to a point on the circumference of the load that is at an angle θ_i with respect to a global coordinate frame, and the orientation of the ant with respect to the normal at that position is ϕ_i (see Fig. 2.1).

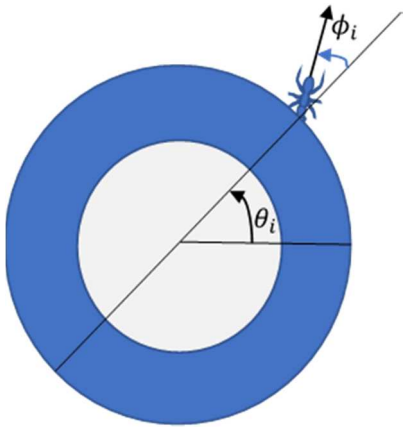

Figure 2.1 Ant Point of Attachment and Orientation on a Load

An attached ant can occupy one of two roles: puller or lifter. A puller attempts to drag the load towards a destination and in doing so, it attempts to align itself with the direction of the force required to achieve this motion. Lifters, on the other hand, lift the cargo in a bid to mitigate the effects of friction.

The model assumes that all ants attached to the load lift with a lifting force $F_l = 2.59\ mN$ and that the load is subjected to a kinetic friction force. Based on this, the normal force F_N on the load can be evaluated by assuming that the load is in vertical equilibrium.

$$F_N = Mg - N_L(t)F_l \qquad \text{Eq (1)}$$

where M = mass of the payload, g = acceleration due to gravity, and $N_L(t) =$ the number of robots occupying the lifting role at time t.

Given that each pulling ant applies a force f_0, the net force acting on the load is given by

$$f_{tot} = N_p(t)f_0 - \mu F_N \qquad \text{Eq (2)}$$

where $N_p(t) =$ the number of ants occupying the pulling role at time t.

During motion, the velocity of the load's center of mass, V_{cm}, and the load's angular velocity, ω, are given by

$$V_{cm} = \frac{f_0 - f_{kin}}{\gamma} \qquad \text{Eq (3)}$$

$$\omega = \frac{\tau_0 - \tau_{kin}}{\gamma_{rot}} \qquad \text{Eq (4)}$$

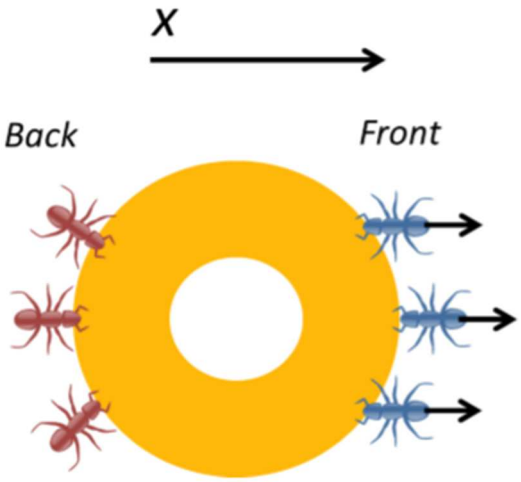

Figure 2.2 Illustration Of Ants Connected To Load (blue ants are pullers, red ants are lifters).

Figure 2.2 is taken from (Gelblum, et al., 2015). The constants γ and γ_{rot} are load response coefficients for an applied force and torque, respectively, given by the expressions:

$$\gamma_{rot} = \frac{I}{\delta t} \qquad \text{Eq (5)}$$

$$\gamma = \frac{M}{\delta t} \qquad \text{Eq (6)}$$

where I = moment of inertia of the payload about its centroid, and δt is an infinitesimally small time period.

From Newton's 2nd law over time period δt, we have:

$$M\frac{\delta v_{cm}}{\delta t} = \gamma \times \delta v_{cm} = f_{tot}$$

$$\delta v_{cm} = \frac{f_{tot}}{\gamma} \qquad \text{Eq (7)}$$

Since the motion of the load occurs over a planar surface, its velocity can be decomposed into the following *x* and *y* components:

$$V_{cm,x} = \frac{f_0 \sum_{i \in N} n_p(\theta_i, \phi_i) \cos(\theta_i + \phi_i) - f_{kin,\ x}}{\gamma}$$

$$V_{cm,y} = \frac{f_0 \sum_{i \in N} n_p(\theta_i, \phi_i) \sin(\theta_i + \phi_i) - f_{kin,\ y}}{\gamma} \qquad \text{Eq (8)}$$

The angular velocity of the load is given by

$$\omega = \frac{f_0 \sum_{i \in N} n_p(\theta_i, \phi_i) \sin(\theta_i) - \tau_{kin,\ y}}{\gamma_{rot}} \qquad \text{Eq (9)}$$

It is reasonable to assume that during a collective transport task, ants have the ability to sense the amount of force that is being exerted on the payload. This local force (f_{loc}^i) varies according to the site of an ant's attachment. The force can be modeled as

$$f_{loc}^i = f_{cm} - f_{rot}^i$$

$$f_{loc}^i = \gamma v_{cm} - \frac{\gamma_{rot}}{b} r_i \times \omega \qquad \text{Eq (10)}$$

where b is the distance from the centroid to the point of the ant's attachment.

2.2 Microscopic Model of Ant Role Selection and Switching

As the ants transport the payload, they switch roles between pulling and lifting. This allows the ants to easily adjust when new information is introduced into the system. (Gelblum, et al., 2015) show that interactions between the ants through the payload can be described using a one-dimensional Ising model. The probabilities of ants entering either state (role) from the other state are modeled as functions of the local force sensed by the ant, and an individuality parameter F_{ind} that determines whether or not the ant chooses to align its force with the load's direction of motion:

$$P_p = \frac{1}{1 + \exp\left(-\frac{p_i . f_{loc}}{F_{ind}}\right)}$$

$$P_l = \frac{1}{1 + \exp\left(\frac{p_i . f_{loc}}{F_{ind}}\right)} \qquad \text{Eq (11)}$$

$$0 < F_{ind} < 10$$

Higher values of F_{ind} result in more independent behavior from the agent, whereas lower values result in a more coordinated motion. The polarization vector p_i relates the local force to the heading of the payload in the global frame. It behaves like a rotation matrix, since the force sensed by the agent is defined in its local frame.

The transition rates, defined as probabilities per unit time, at which the ants switch from one state to the other can be quantified as:

$$R_{l \to p} = K_c \exp\left(\frac{p_i . f_{loc}}{F_{ind}}\right)$$

$$R_{p \to l} = K_c \exp\left(-\frac{p_i . f_{loc}}{F_{ind}}\right) \qquad \text{Eq (12)}$$

where K_c is the base state transition rate of the system.[2]

2.3 Macroscopic Model of Ant Behavioral Dynamics

In (Pavlic, et al., 2016), the encounters and interactions between agents and the payload are modeled as a chemical reaction network (CRN). The main design parameters are the (p_b, p_u) pair that produce a desired equilibrium allocation of robots around the payload, where p_b is an agent's probability of binding (attaching) to an unoccupied region

[2] More information on the derivations of equations (3)-(12) can be found in (Gelblum, et al., 2015) and (Feinerman, et al., 2018).

of the load (called an "unbound zone"), and p_u is an agent's probability of unbinding (detaching) from the load. The CRN is described by

$$r + U \xrightarrow{p_b e_u} B \qquad \text{Eq (13)}$$

$$r + B \xrightarrow{p_u e_b} U + 2r \qquad \text{Eq (14)}$$

This model divides the payload into bound and unbound zones. Eq (13) represents the event during which a free (unattached) agent, denoted by *r*, encounters an unbound zone on the load, denoted by *U*, at the encounter rate e_u and binds (attaches) to this unbound zone with a mass-action rate of $p_b e_u$ to generate a "bound zone". Eq (14) represents the other event, during which a free agent encounters a bound zone, denoted by *B*, at the encounter rate e_b. In this case, the presence of the free agent triggers the attached agent to detach with a mass-action rate of $p_u e_b$, giving rise to two free agents and one unbound zone.

The macroscopic (or mean-field) model describing the population dynamics of a swarm of agents that follow the behaviors described by this CRN takes the form of a set of first-order ODEs, in which *r, U,* and *B* now represent the expected populations of the free agents, unbound zones, and bound zones as continuous functions of time:

$$\begin{bmatrix} \dot{r} \\ \dot{U} \\ \dot{B} \end{bmatrix} = (p_u e_b r B - p_b e_u r U) \begin{bmatrix} 1 \\ 1 \\ -1 \end{bmatrix} \qquad \text{Eq (15)}$$

Assume that the initial number of free agents, r_0, and the initial number of bound agents, B_0, are such that $r_0 + B_0 > B^*$, where B^* is the equilibrium concentration of bound zones. Then this approach is shown to produce, on average, a target equilibrium allocation of agents around the payload such that (Pavlic, et al., 2016):

$$\frac{B^*}{U^* + B^*} = \frac{1}{1 + \delta} \frac{\frac{p_b}{p_u}}{\frac{p_b}{p_u} + \frac{e_b}{e_u}} \quad \text{Eq (16)}$$

where δ is a correction factor that accounts for spatial effects on the load boundary in a physical robot scenario.

3 CONTROLLER AND SIMULATION SETUP

3.1 Model Assumptions

3.1.1 Sensory Capabilities

We assume that the agents are informed of their position coordinates in a global frame. While searching for the load, agents move with a sensory cone that gives them an awareness of the environment. We also assume that agents can access the coordinate locations of entities they encounter within the environment such as nests or waypoints. The agents are also able to sense when a leader is attached to the payload.

3.1.2 Communication Capabilities

Typical models of swarms are based on the fundamental assumptions that agents act independently and do not communicate with each other. We apply the same assumptions and operate under the assumption that the agents in our case also do not communicate with each other. The only exceptions to this rule are the leaders which are able to broadcast destination information to the rest of the team when the attached to the load.

Our collective transport approach incorporates a leader-follower strategy that allows one agent to influence the overall behavior of the transport team. This is aptly summarized in (Gelblum, et al., 2015):

"By combining the analysis of the load motion with single-ant trajectory data, we find that while the combined force of the group determines the speed of the load, it is individual informed ants that steer the direction of movement."

With this is mind, leader agents are given the ability to communicate desired destinations to the other team members. This communication is restricted to the agents attached to the load at the same time as the leader.

3.1.3 Role Definitions

Agents attached to a load may adopt particular roles, such as pullers and lifters, based on their position on the load relative to the direction of transport motion. However, in this work, we treat these roles as functions of the force the agent can sense is being exerted on the load by other agents also attached to the load.

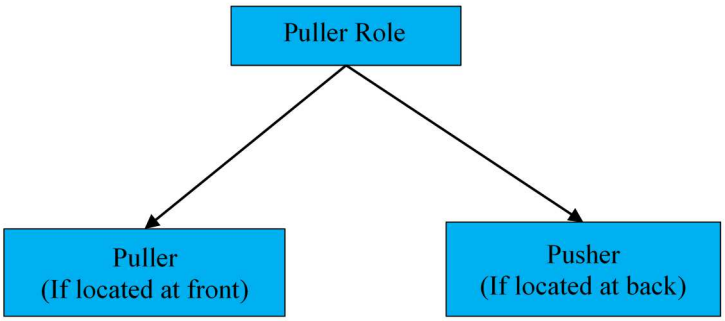

Figure 3.1 Redefinition of Puller Role

Given this, we redefine the puller role from (Feinerman, et al., 2018) as two subtasks of pulling and pushing (Fig. 3.1). In our model, agents classified as pullers in (Feinerman, et al., 2018) that occupy positions on the back of the load will instead apply a pushing force of the same magnitude and direction as the pulling force. This prevents agents from positioning themselves underneath the payload, since an agent that applies a pulling force to the load while attached to the back of the load would have to be underneath the load. Agents that occupy either of these roles will be referred to as puller agents.

3.2 Stochastic Controller Design

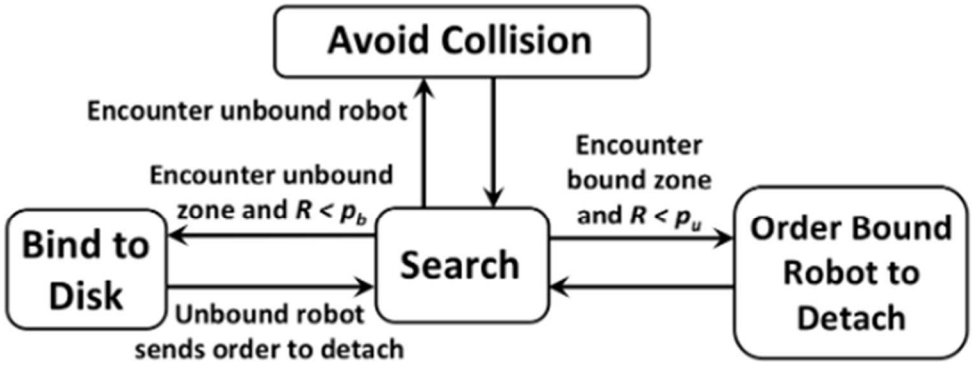

Figure 3.2 Control Flow Diagram of Stochastic Model from (Pavlic, et al., 2014). *R* is a random value drawn from a uniform distribution with parameters ($\mu = 0, \sigma = 1$)

Agents exhibit three types of behaviors during the entire transport process:

1. Search – Agents are initially not attached to a payload. They roam the environment following a correlated random walk (CRW) motion model. This means that the agents move forward for a unit time step and then make a turn through a random angle. The agent repeats this action indefinitely, while also maneuvering to avoid collisions with other agents. Agents that exhibit this behavior are called *free agents*.
2. Agent-load interactions – These describe the agent response to encountering a payload. Once an agent senses a payload, it moves towards it and decides to attach itself or not. The agent will attach itself with a probability of p_b. Once

an agent binds to the payload, a "bound zone" is created. Otherwise, the agent fails to bind and continues its correlated random walk.

However, if an agent is designated as being informed of the desired destination then it attaches itself to the payload without fail. This dynamic exists in the scenario described later in section 3.4.2.

3. Agent-agent interactions – As an agent performs its CRW, it may encounter another agent that is also in the search phase. In this case, both agents perform a maneuver to avoid collision.

   An agent may also find another agent has already attached itself to an attachment zone (creating a bound zone). In this case, the free robot commands the bound robot to detach from the payload with a probability p_u. Otherwise, the free robot just turns and continues its CRW. Equivalently, the bound robot can detach from the payload with probability p_u upon sensing the presence of a free robot nearby.

These three behaviors can be described by a finite state machine with four states, shown in Fig. 3.2: search, avoid collisions, bind to load, and order bound robot to detach. Transitions from one state to another are triggered by the conditions shown in the figure.

3.3 Puller-Lifter Transition Controller

Robots attached to the payload (bound robots) occupy one of the two roles described previously, lifter and puller, and transition between the two roles throughout the transport, as described by the following chemical reaction model:

$$Lifter \rightleftharpoons Puller \qquad \text{Eq (16)}$$

These transitions occur at a mass action rate $R_{p\to l}\ P_L$ for the forward reaction and $R_{l\to p}\ P_p$ for the backward reaction.

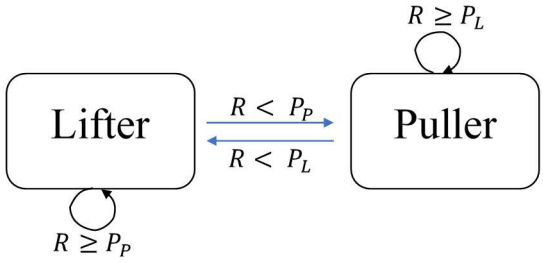

Figure 3.3 Finite State Machine Representation of Role Selection. R is a random value drawn from a uniform distribution with parameters ($\mu = 0, \sigma = 1$)

3.4 Force Controller

In (Kumar, et al., 2013), experimental data on ants performing a collective transport task showed that the ants move the load at approximately a constant velocity. To this end, the model in this work uses a simple proportional controller to regulate the value of each agent's pulling force:

$$F_p = K\ (v_L^d - \ v_L) \qquad \text{Eq (17)}$$

where v_L^d is the desired load velocity, and v_L is the actual load velocity.

3.5 Simulation Setup

The simulations were run in Netlogo (Wilensky, 1999). The code for the simulations was based on the code used to produce the agent-based simulations from (Pavlic, et al., 2014). In the code, the robot role selection procedure presented in that paper

was changed to the one described in Section 3.3. The payload to be transported is a coin and the robots were simulated as ants, since they are the inspiration for this work.

Simulations were run for two scenarios:

1. Scenario 1 - Load transport to a target destination that is known by all the robots
2. Scenario 2 - Leader-follower transport with periodically updated target destinations determined by temporary "leader" robots attaching to the load

3.5.1 Scenario 1

In scenario 1, all robots have knowledge of the nest position, which is the target destination for the load. The task then becomes working together to transport the payload to the desired location. The ants rely only on information they acquire during their search phase to execute the transport task.

Table 3-1 Design of Experiment for Scenario 1

Experiment	Spontaneous Detachment Rate (Hz)	Role Selection Based on Force Sensed by Robot on Load	Role Selection Based on Robot Location on Load
1	0.13	Yes	No
2	0	Yes	No
3	0	No	Yes
4	0.13	No	Yes

In Table 3-1, we have the setup for the experiments to be run for scenario 1. The main parameters to explored are the effects of the role selection procedure proposed in section 3.3 and spontaneous agent detachment from the load on the system. Column 1 of the table indicates whether agent detachments from the payload occur by means of the

catalytic reaction in equation (14) (in this case, the rate is 0), or by spontaneous detachment (in this case, the rate is positive). Columns 2 and 3 indicate the role update procedure that is being employed.

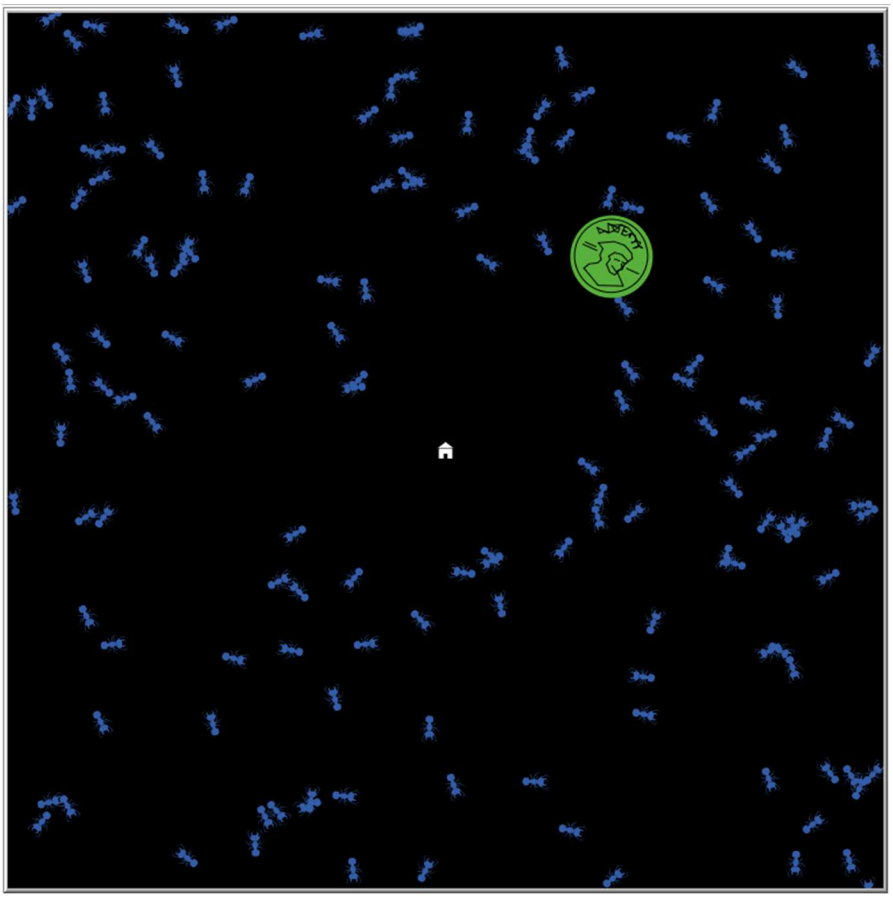

Figure 3.4 Simulation Environment Setup for Scenario 1. Blue ants are free ants executing the search phase; white house icon is nest location.

3.5.2 Scenario 2

In scenario 2, the robots start with different ideas of where the target destination is. Each robot selfishly attempts to move the payload to its own preprogrammed destination coordinates. Free robots behave as scouts to identify the coordinates of a waypoint, defining a target location for the load along the way to the nest, and the nest itself. Once a

scout discovers a waypoint or the nest, it is designated as a potential leader for the transport team. During the transport, a leader robot may join the robot team and update the destination coordinates of the team. Communication only occurs between the leader and the rest of the robot team. The remaining team members are unable to communicate with one another.

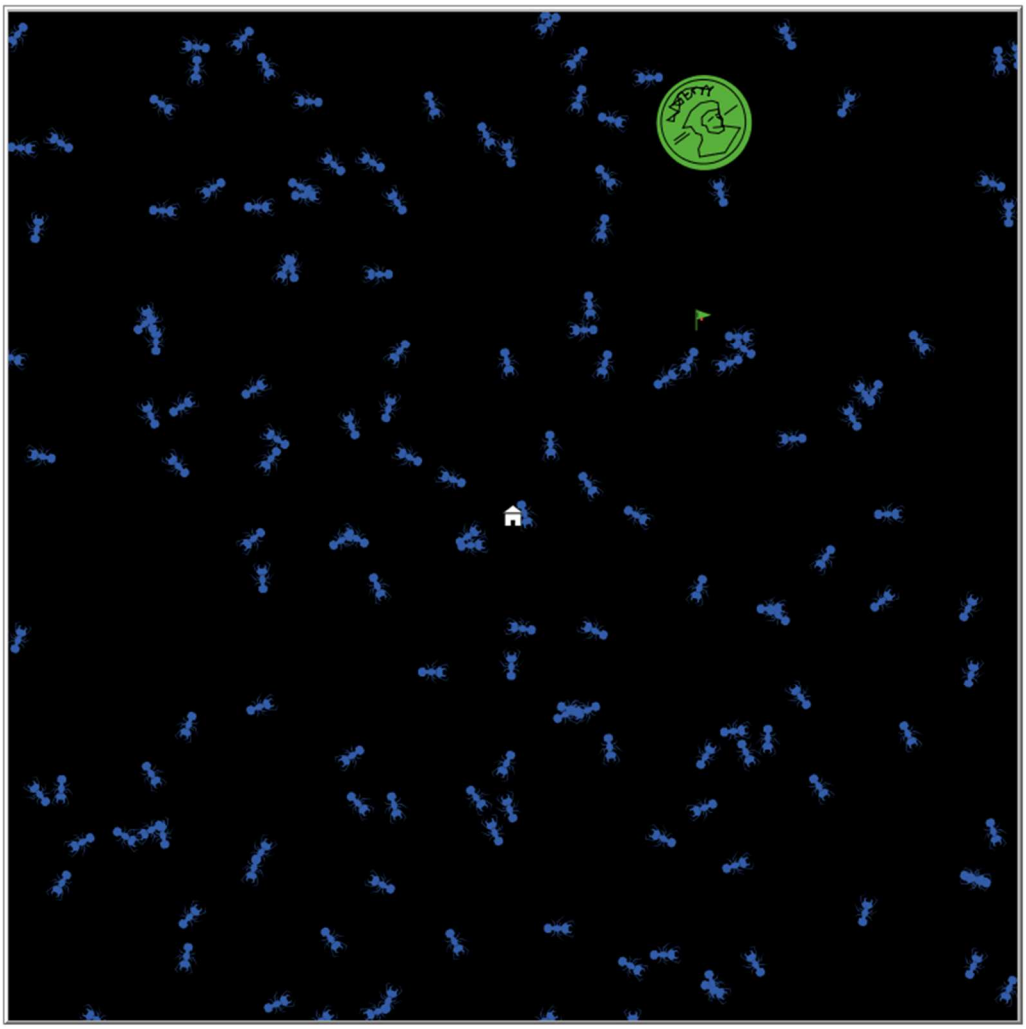

Figure 3.5 Simulation Environment Setup for Scenario 2. Green flag icon denotes a waypoint; white house icon is nest location.

The waypoint position is pseudo-randomly generated to be located between the coin starting point and the final destination (nest). Robots can determine the coordinates of the waypoint when they encounter it, becoming informed robots and potential leader robots.

When there are multiple informed robots attached to the load, the leader is then the agent that is farthest from its target coordinate. Because of this, having multiple informed robots that have the same information should have no significant effect on the system.

Table 3-2 Design of Experiment for Scenario 2

Experiment	Spontaneous Detachment Rate (Hz)	Role Selection Based on Force Sensed by Robot on Load	Role Selection Based on Robot Location on Load	Informed Robots Forget Destination Coordinates
1	0.13	Yes	No	Yes
2	0.13	Yes	No	No
3	0.13	No	Yes	No
4	0.13	No	Yes	Yes

As shown in Table 3-2, the design of experiments for scenario 2 focuses on the effects of the role selection procedure used, and whether or not the informed robots eventually forget the load destination. Where relevant (as determined by column 4 of Table 3-2), the informed robots lose their coordinate information after a random time drawn from an exponential distribution.

Table 3-3 Simulation Parameters

Parameter	**Value**
Coin mass (M)	3.1 g

Coin radius (r)	8.5 mm
Number of robots (r_0)	150
Robot length	0.8 cm
Robot sensing cone	$angle = 180°$ $length = 0.13\ cm$
Friction coefficient (μ)	0.59
Robot lifting force (F_L)	2.59 mN
Probability of attachment (p_b)	1
Probability of detachment (p_u)	0.5
Spontaneous detachment rate	$\begin{cases} 0.13\ Hz & ,if\ spontaneous\ detachment \\ 0\ Hz & ,if\ no\ spontaneous\ detachment \end{cases}$
Stopping distance from destination	0.3 cm
Desired load velocity (v_L^d)	0.35 cm/s
Simulation time step (dt)	0.01 s
Rate of forgetting waypoint coordinates	$\begin{cases} 0.14\ Hz & ,if\ forgetting\ included \\ 0\ Hz & ,if\ no\ forgetting \end{cases}$
Rate of forgetting nest coordinates	$\begin{cases} 0.1\ Hz & ,if\ forgetting\ included \\ 0\ Hz & ,if\ no\ forgetting \end{cases}$

Table 3-3 contains the parameters that are used to setup and run the simulations. These remain constant for all simulations to ensure consistency in the simulations.

4 SIMULATION RESULTS

For each experiment listed in Tables 3.1 and 3.2, 30 simulation trials were run in NetLogo. In the plots below, the black line shows the average over these 30 simulations, and the shaded region indicates the range of +/- one standard deviation.

4.1 Scenario 1

This scenario considered the case where all robots are informed of the destination and just work together to move the load from its initial position to its destination.

Results of Experiment 1

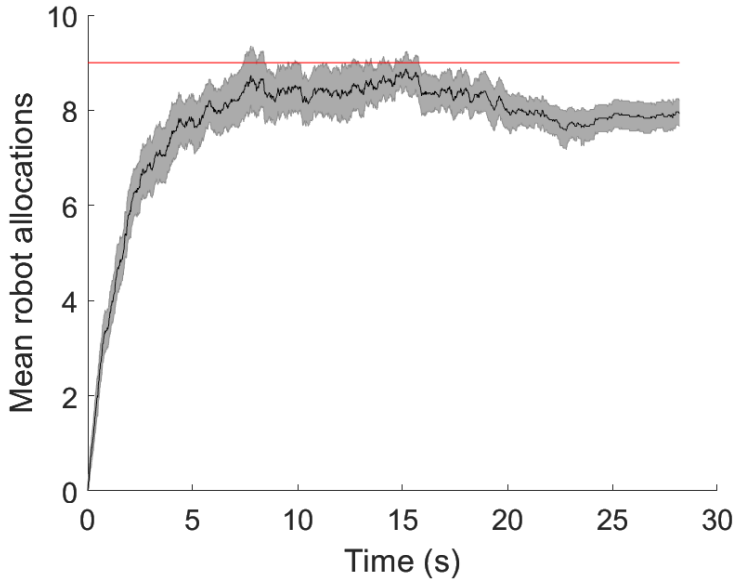

Figure 4.1 Mean Robot Allocation over Time. Red line shows the target robot allocation around the payload

Figure 4.1 shows the number of robots that attach to the payload over time and are involved in the transport task during experiment 1. From this figure, we observe that the mean number of robots approaches the target allocation value ($\approx 9\ robots$) although there is some significant deviation throughout the transport.

In Figure 4.2, we observe that the payload begins significant displacement after about 5 s have passed. A comparison between at Figures 4.1 and 4.2 reveals that motion truly begins when the number of robots attached to the payload exceeds 5.

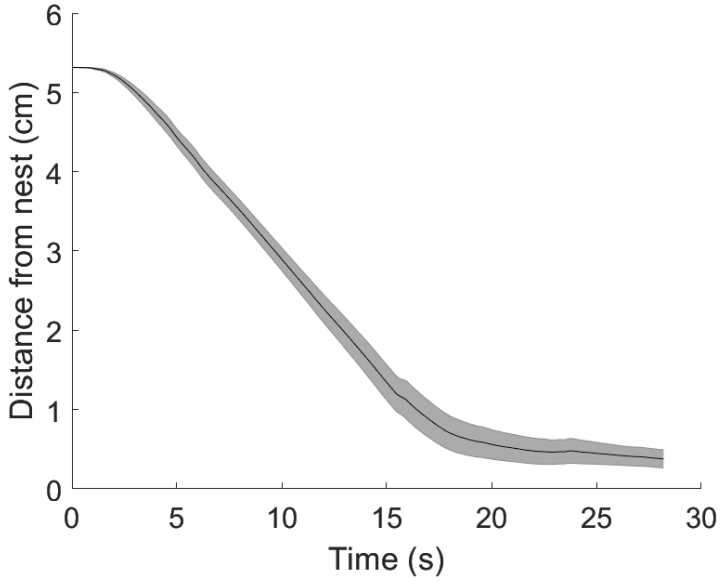

Figure 4.2 Distance of Load from Destination over Time. Stopping distance is 0.3 cm

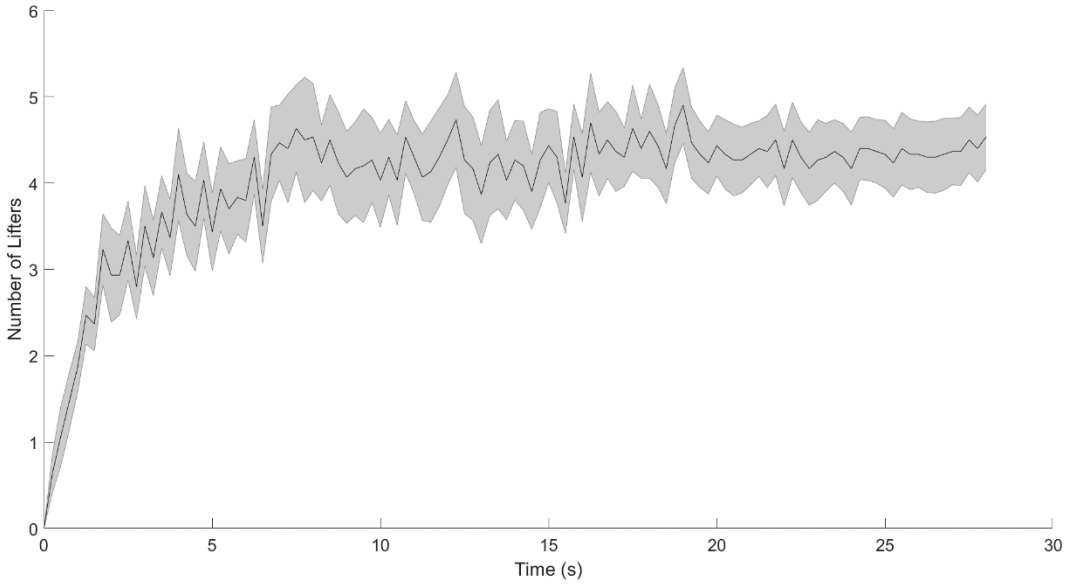

Figure 4.3 Time Evolution of Number of Robots in Lifting Role, Sampled over Time Intervals of 0.25 seconds.

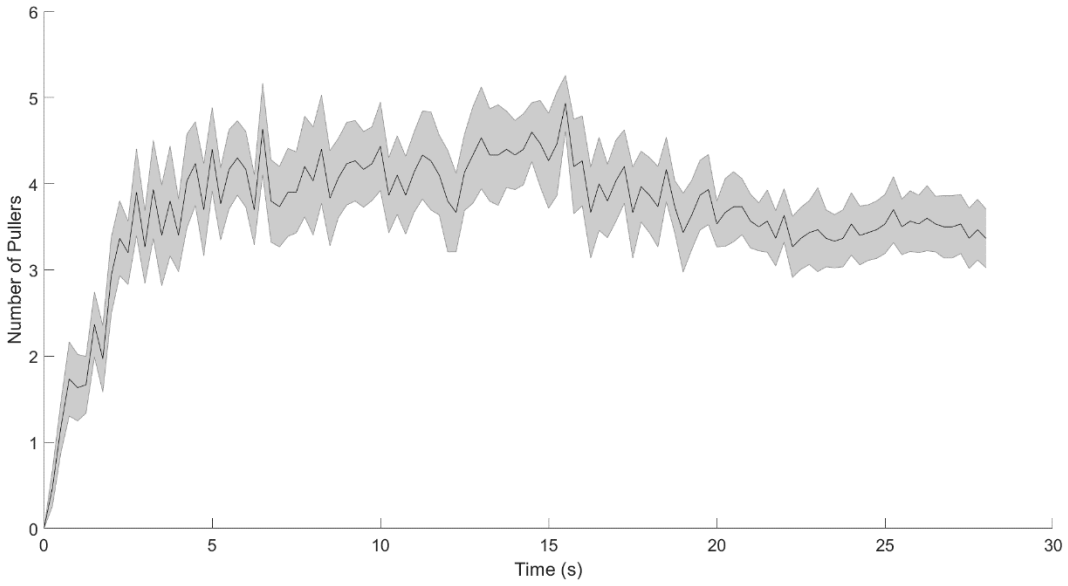

Figure 4.4 Time Evolution of Number of Robots in Pulling Role, Sampled over Time Intervals of 0.25 seconds.

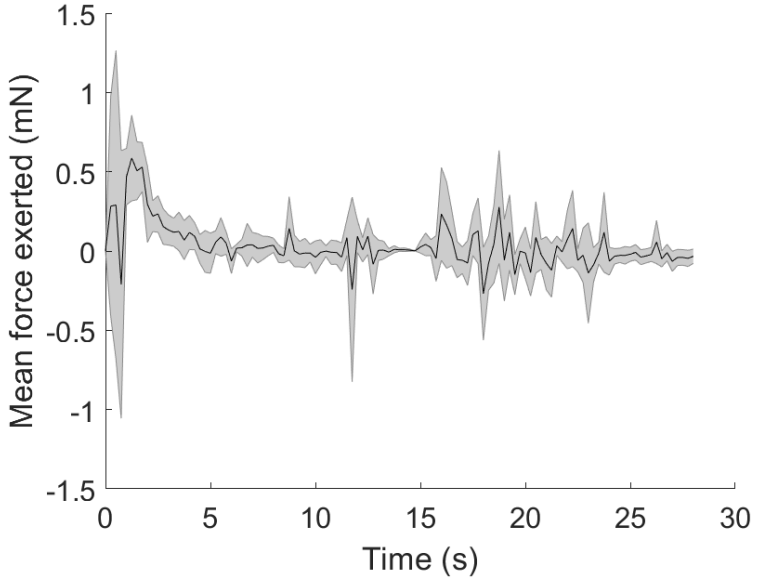

Figure 4.5 Mean Value of Force Magnitude Exerted by Each Robot on the Payload. Values are sampled at 0.25 second intervals

Throughout the transport, the robots are observed to constantly switch between puller and lifter roles. However, in Figure 4.3 and 4.4 we observe that the number of robots

in each role approaches about half the population of the current transport team. Figure 4.5 shows that the payload experiences a significant amount of force in the beginning of the transport task. As the transport progresses, the number of robots attached to the load increases (with robots allocating themselves relatively uniformly around the load), and thus the robots must individually exert less force to transport the load at the same velocity. This phenomenon is shown in Figure 4.5. After some fluctuation, the force plot begins to approach zero as the velocity approaches the desired velocity of 0.35 cm/s, as seen in Figure 4.6. During this phase, the transport team behaves like a system in dynamic equilibrium as the force balance is achieved. This is however easily disrupted when there are sudden spikes in the force, as seen in Figure 4.5. The spikes in forces exerted are reflected in the load velocity, shown in Figure 4.6, where this velocity is seen to exceed the desired value at around t = 15 s. During the simulations, these spikes corresponded with changes in load direction or imbalance in robot allocation around the load.

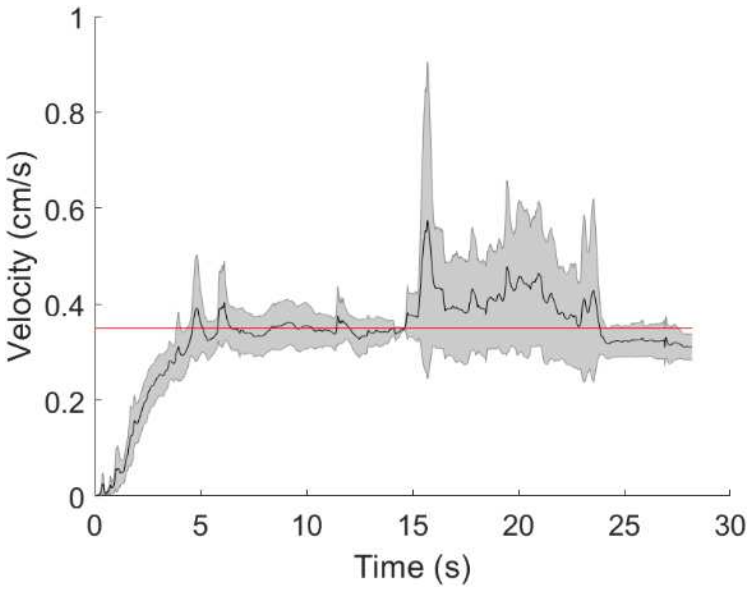

Figure 4.6 Speed of Payload over Time under Action of Forces Exerted by the Attached Robots. Red line shows desired load velocity, 0.35 cm/s.

Table 4-1 Comparison of Experiment Results for Scenario 1

Parameter	Experiment 1	Experiment 2	Experiment 3	Experiment 4
Mean number of robots attached to the load	7.2270	8.9675	9.4570	8.1414
Mean number of pullers	3.6929	4.4437	1.7927	1.6071
Mean number of lifters	4.0298	4.5237	7.6647	6.5342
Mean force exerted by robots on the load	0.0524 mN	0.0327 mN	0.1290 mN	0.1606 mN
Mean load velocity during transport	0.3829 cm/s	0.3201 cm/s	0.3204 cm/s	0.3063 cm/s

The values in Table 4-1 are average values taken over 30 simulation runs for each experiment. First, the mean values over time were calculated and then a mean was taken over the number of simulations. From the table, we observe that for the experiments that implemented the role selection based on the forces sensed by the agents, the mean ratio of pullers to lifters over the course of the transport is almost 1:1. Thus, the robots that attach to the payload distribute into two groups of almost equal size.

We also observe significantly reduced force magnitudes being exerted by the robots in Experiments 1 and 2, compared to Experiments 3 and 4. Although the robots transport the payload with almost similar velocities, we see that the load forces required to achieve this motion are greatly reduced in Experiments 1 and 2.

Results from Experiment 2-4 are plotted in Appendix A.

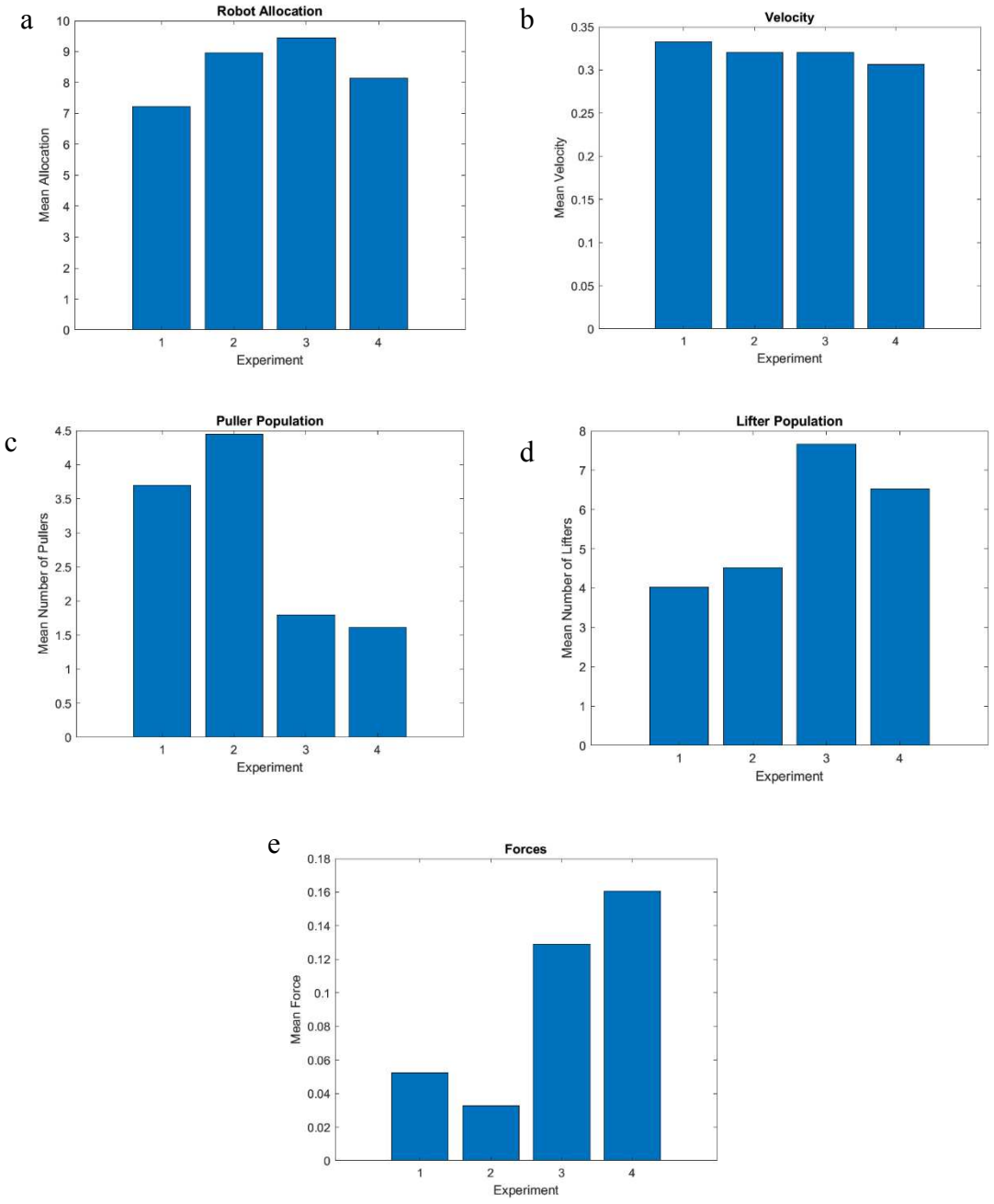

Figure 4.7 Bar Plots of Mean Values Shown in Table 4-1.

4.2 Scenario 2

In this scenario, each robot is initialized with randomly generated destination coordinates. This information on the destination is updated only when a leader robot joins the transport team.

Results of Experiment 1

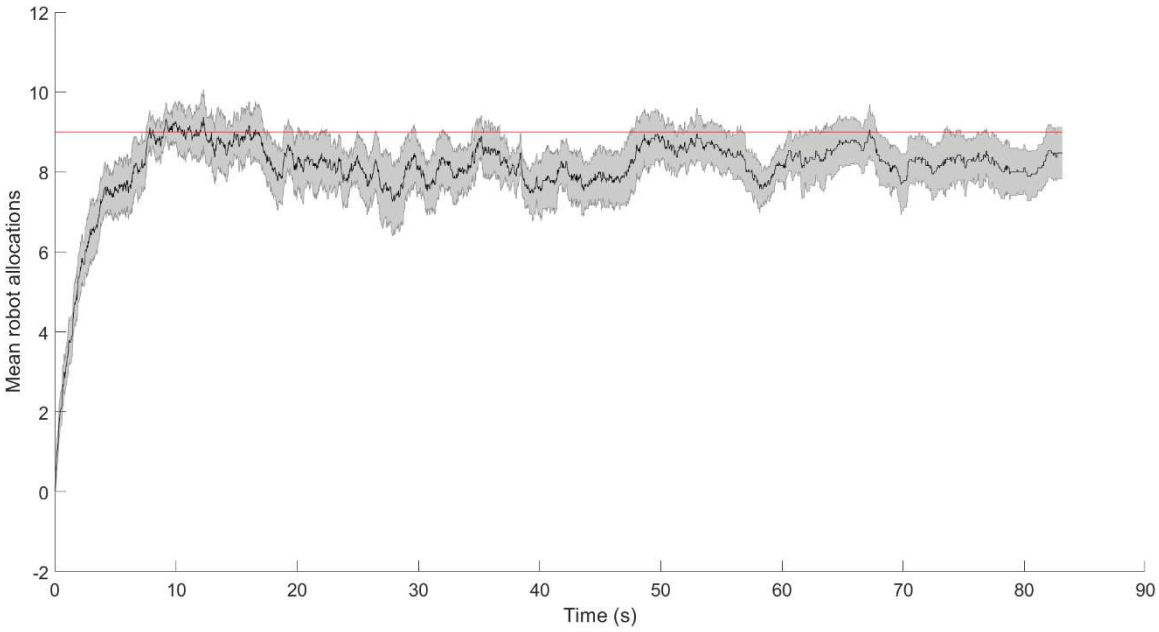

Figure 4.8 Mean Robot Allocations over Time. Red line shows the target robot allocation around the payload (target ≈ 9)

In Figure 4.8, we observe that the robot allocations around the payload fall just short of the target allocation value. We observe the increase in allocation values shows a direct correlation with displacement; significant displacement of the payload begins after the number of attached robots reaches 6, shown in Figure 4.9. We also observe the number of agents in each role approaches about half of the transport team population.

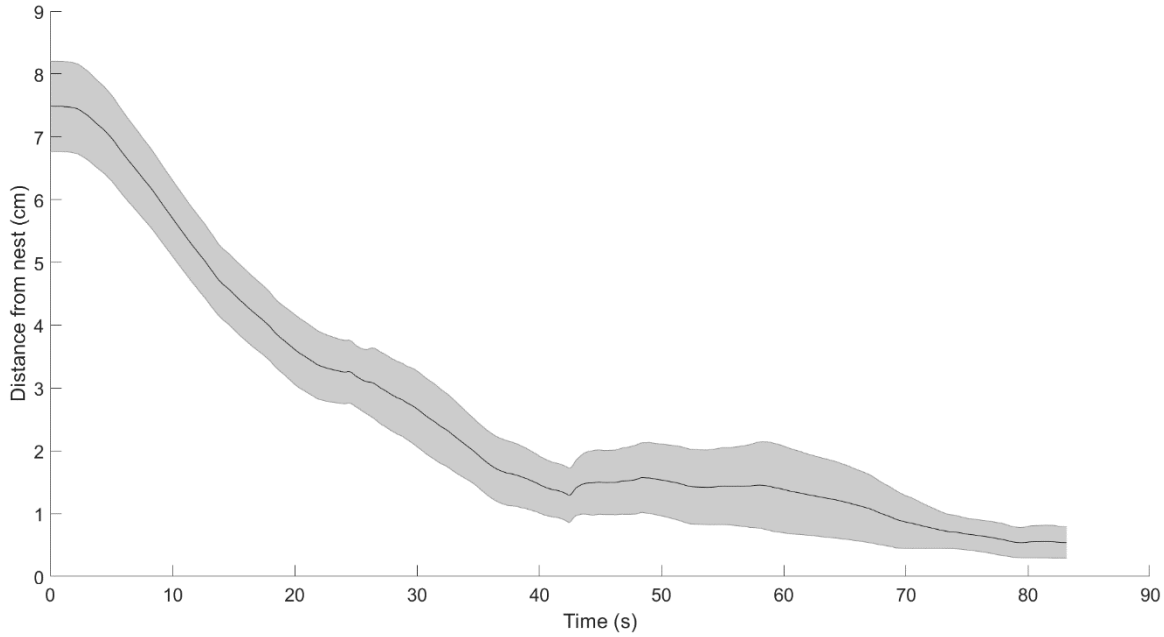

Figure 4.9 Distance of Load from Destination over Time. Stopping distance was 0.3 cm

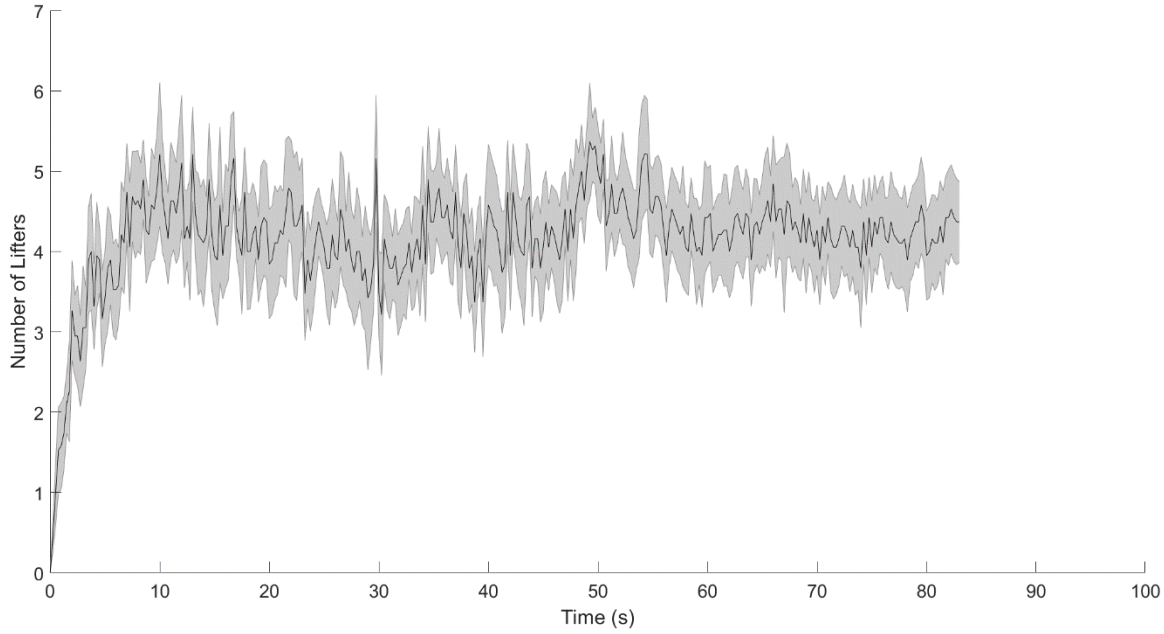

Figure 4.10 Time Evolution of Number of Robots in Lifting Role, Sampled over Time Intervals of 0.25 seconds.

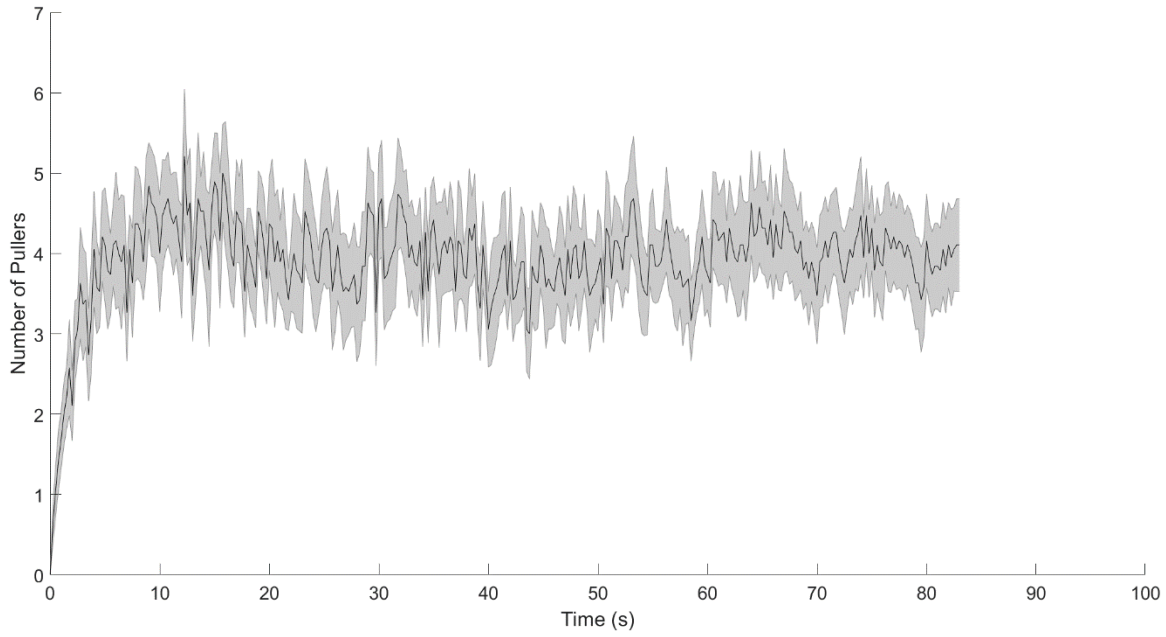

Figure 4.11 Time Evolution of Number of Robots in Pulling Role, Sampled over Time Intervals of 0.25 seconds.

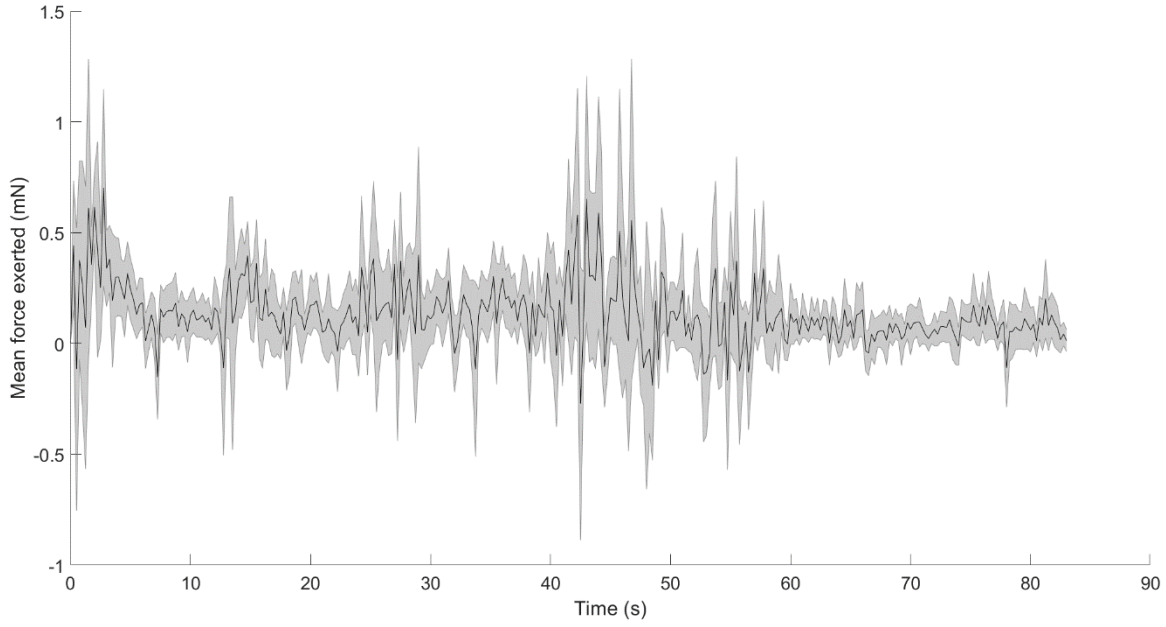

Figure 4.12 Mean Value of Force Magnitude Exerted by Each Robot on the Payload. Values are sampled at 0.25 second intervals.

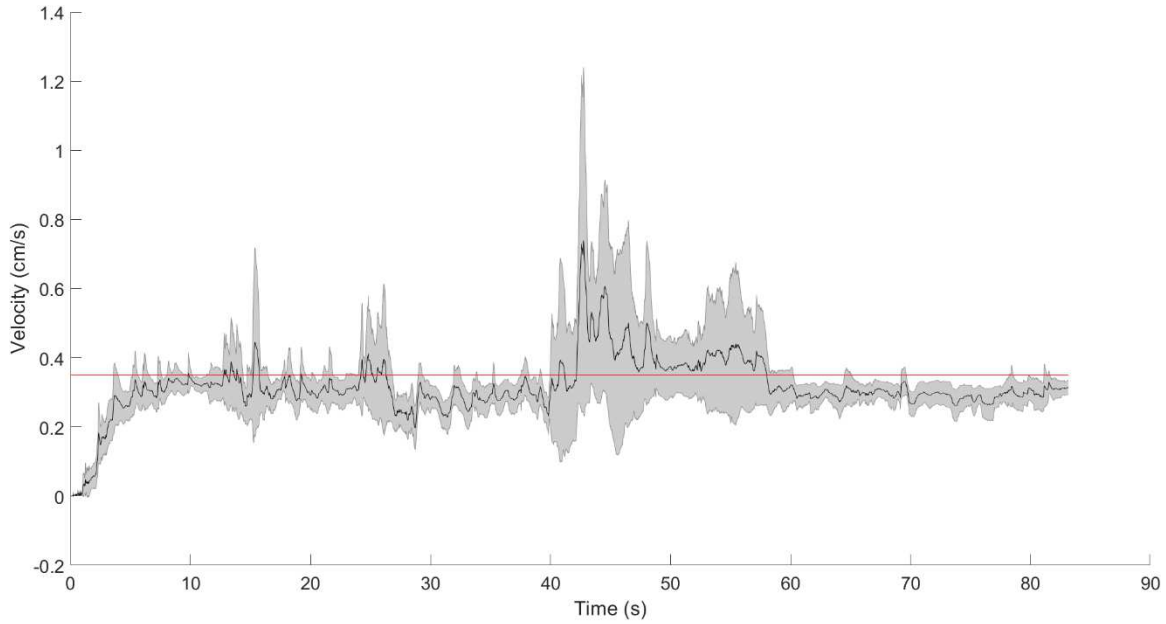

Figure 4.13 Speed of Load over Time under Action of Forces Exerted by the Attached Robots.

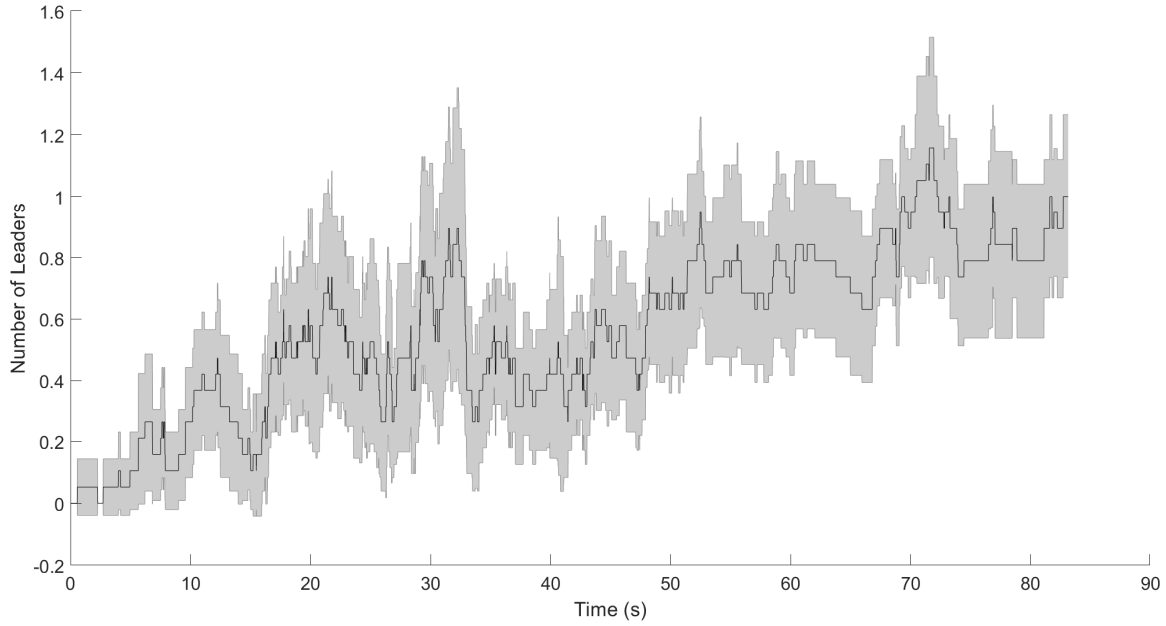

Figure 4.14 Mean Number of Informed Robots Attached to Payload

In Figure 4.14, we see that the mean number of informed robots that attach to the payload increases as the total number of informed agents also increase, shown in Figures

4.15 and 4.16. This attachment event is however relatively low compared to the attachment of uninformed robots.

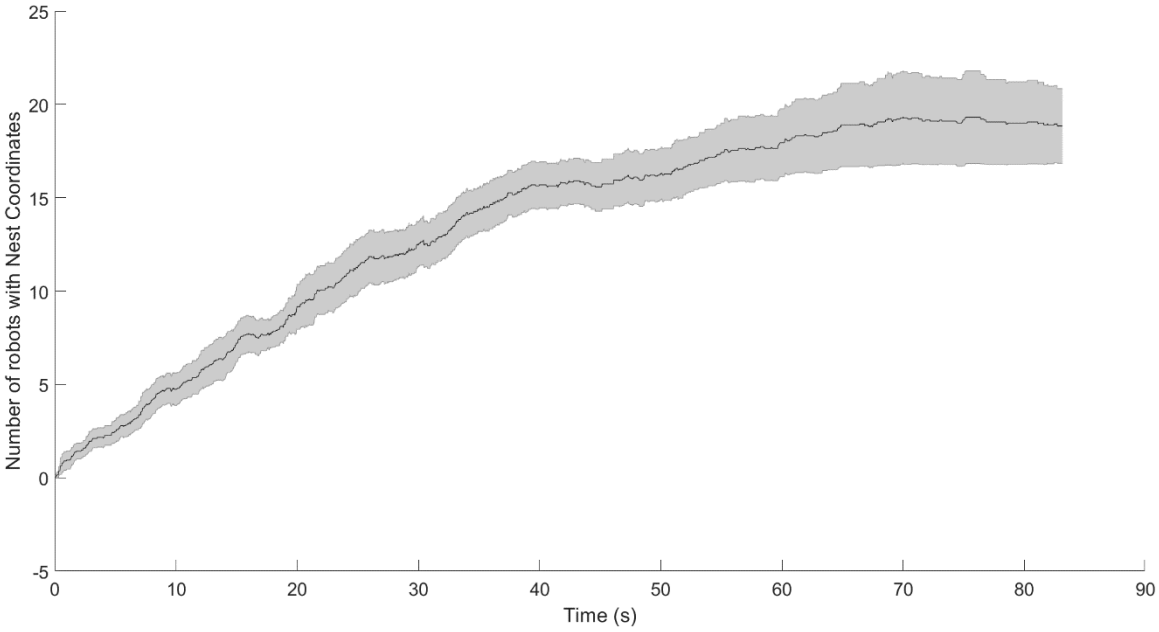

Figure 4.15 Mean Number of Robots Informed with Nest Coordinates

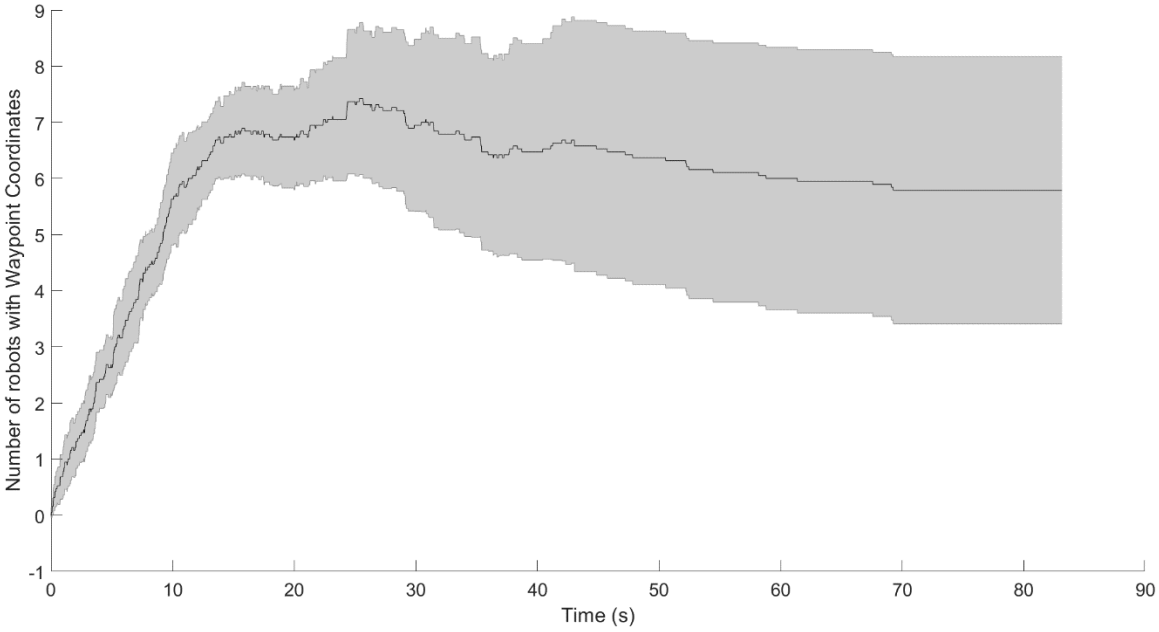

Figure 4.16 Mean Number of Robots Informed with Waypoint Coordinates

Table 4-2 Comparison of Experiment Results for Scenario 2

	Experiment 1	Experiment 2	Experiment 3	Experiment 4
Mean number of robots attached to the load	8.1020	8.0789	8.6389	8.6294
Mean number of pullers	4.0412	4.0136	1.9637	2.0173
Mean number of lifters	4.0572	4.0621	6.6752	6.5961
Mean force exerted by robots	0.1216 mN	0.1055 mN	0.3862 mN	0.2996 mN
Mean Number of Robots Informed with Waypoint Coordinates	5.5685	7.3519	6.4272	6.3918
Mean Number of Robots Informed with Nest Coordinates	13.8766	15.1928	13.6084	14.8937
Number of leader robots	0.6040	0.5959	0.4731	0.3591
Mean load velocity during Transport	0.3228	0.3264	0.2810	0.3219

The values in Table 4-2 were computed similarly to the values in Table 4-1. From Table 4-2, the force expenditure benefits significantly from the role update procedure based on forces sensed. Under this policy, the main trend that can be noticed is that the ratio of pullers to lifters is 1:1. The mean force exerted on the payload by each agent in Experiments 1 and 2 is also significantly reduced from the forces exerted in Experiments 3 and 4.

The spontaneous forgetting condition has little effect on the numbers of informed robots. Instead, the role update procedure shows the greatest effect on the results. The mean robot allocation throughout the transport is seen to be relatively equal across all experiments. We also see relatively similar transport speeds across the experiments. However, as can be seen in Figure 4.17, the magnitudes of forces exerted under the force-based role update procedure are significantly lower than under the position-based role update procedure.

Results from Experiment 2-4 are plotted in Appendix B.

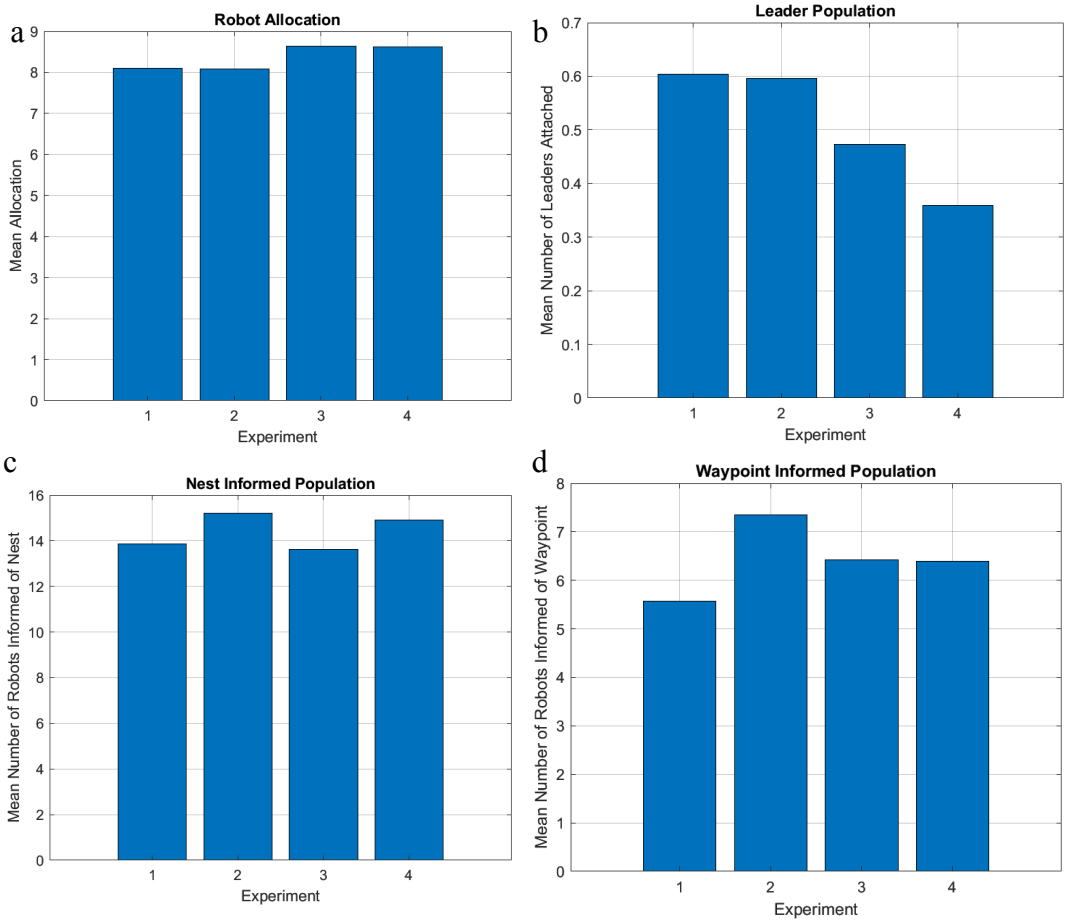

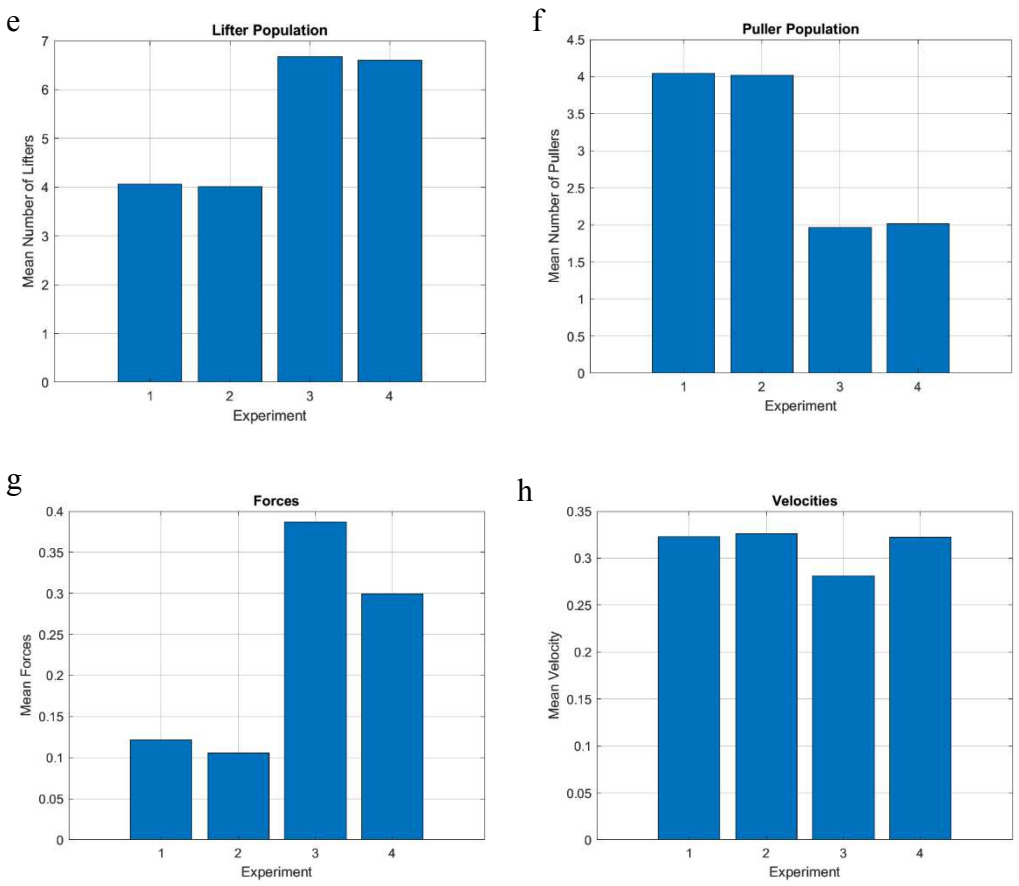

Figure 4.17 Bar Plots of Mean Values shown in Table 4-2.

5 CONCLUSION AND FUTURE WORK

5.1 Conclusion

This thesis explores the effect of a force-based role update procedure on collective transport. The thesis presents the kinematics and dynamics of an agent-load system during collective transport. In this thesis, an investigation was made into the effect of informed robots that act as temporary "leaders," searching an environment for a destination point and transmitting that information to a robot team to guide the transport to this destination. The system was modeled in NetLogo and agent-based simulations were run for different scenarios. From the simulations, we can draw the following conclusions.

Updating the roles of the robots based on the forces sensed produces an approximately 1:1 allocation of roles. By employing the role selection algorithm, about half the robots tend to choose the puller role, and the other half become lifters. This is found to be the case even when the robots have different target coordinates.

Experimental results also show that the force-based role update procedure results in less force input demand from the members of the robot team than role updates based on robots' positions around the load. This can serve as a basis for designing robot controllers that obey physical constraints on the robots' maximum applied forces on the load.

5.2 Future Work

Future expansion of this work could investigate a model where communication does not occur between the robots at all. In our model, communication is enabled for the leader robots to communicate the destination information to the rest of the robot team. This is a departure from the observation that ants do not actually communicate explicitly during collective transport.

The model could also be expanded to describe different attachment and detachment behaviors for the informed robots. In our current model formulation, the informed robots follow the same behavioral rules as the uninformed robots. In practice, one would expect that the informed robot gives greater priority to joining the robot team and updating the destination coordinates.

Our model is also not constrained to sequentially follow a set of waypoints. The probability that the robots carry the load to a particular destination is dependent on the attachment of an informed ant with knowledge of that destination. Future work could focus on programming the robots to sort through the destination information and follow a sequence of coordinates.

REFERENCES

Berman, S. et al., 2011. *Study of group food retrieval by ants as a model for multi-robot collective transport strategies.* Los Angeles, MIT Press, pp. 259-266.

Bonabeau, E., Dorigo, M. & Theraulz, G., 1999. *Swarm Intelligence: From Natural to Artificial Systems.* New York: Oxford University Press.

Brambilla, M., Ferrante, E., Biratti, M. & Dorigo, M., 2013. Swarm robotics: a review from the swarm engineering perspective. *Swarm Intelligence,* 7(1), pp. 1-41.

Feinerman, O. et al., 2018. The physics of cooperative transport in groups of ants. *Nature Physics,* 14(7), pp. 683-693.

Gelblum, A. et al., 2015. Ant groups optimally amplify the effect of transiently informed individuals. *Nature Communications,* 28 July, 6(1), p. 7729.

Gelblum, A. et al., 2016. Emergent oscillations assist obstacle negotiation during ant cooperative transport. *Proceedings of the National Academy of Sciences,* 113(51), pp. 14615-14620.

Kube, R. C. & Bonabeau, E., 2000. Cooperative transport by ants and robots. *Robotics and Autonomous Systems,* 31 January, 30(1-2), pp. 85-101.

Kumar, G. P., 2016. *Development and Analysis of Stochastic Boundary Coverage Strategies for Multi-Robot Systems,* Ph.D Thesis: Arizona State University.

Kumar, G. P. et al., 2013. A stochastic hybrid system model of collective transport in the desert ant Aphaenogaster cockerelli. *International Conference on Hybrid Systems: Computation and Control (HSCC)*, p. 119–124.

Leucht, K. W., 2015. *NASA, Engineering, and Swarming Robots.* [Online] Available at: https://ntrs.nasa.gov/archive/nasa/casi.ntrs.nasa.gov/20150021902.pdf

Martel, S. et al., 2009. Flagellated Magnetotactic Bacteria as Controlled MRI-trackable Propulsion and Steering Systems for Medical Nanorobots Operating in the Human Microvasculature. *The International Journal of Robotics Research,* 28(4), pp. 571-582.

Pavlic, T. P., Wilson, S., Kumar, G. P. & Berman, S., 2014. Control of Stochastic Boundary Coverage by Multi-robot Systems. *ASME Journal of Dynamic Systems, Measurement, and Control,* 21 October.137(3).

Pavlic, T. P., Wilson, S., Kumar, G. P. & Berman, S., 2016. An Enzyme-Inspired Approach to Stochastic Allocation of Robotic Swarms Around Boundaries. In: *Robotics Research: The 16th International Symposium ISRR.* Singapore: Springer International Publishing, pp. 631-647.

Rubenstein, M. et al., 2013. *Collective Transport of Complex Objects by Simple Robots: Theory and Experiments.* Saint Paul, International Foundation for Autonomous Agents and Multiagent Systems, p. 47–54.

Seyfried, J. et al., 2005. The I-SWARM Project: Intelligent Small World Autonomous Robots for Micro-manipulation. In: *Swarm Robotics.* Berlin: Springer Berlin Heidelberg, pp. 70-83.

Werfel, J., 2012. Collective Construction with Robot Swarms. In: *Morphogenetic Engineering: Toward Programmable Complex Systems.* Berlin: Springer Berlin Heidelberg, pp. 115-140.

Wilensky, U., 1999. *Netlogo,* Evanston: Northwestern University.

Wilson, S. et al., 2014. Design of ant-inspired stochastic control policies for collective transport by robotic swarms. *Swarm Intelligence,* December, 8(4), pp. 303-327.

APPENDIX

A. PLOTS OF EXPERIMENTAL RESULTS FOR SCENARIO 1

Results of Experiment 2

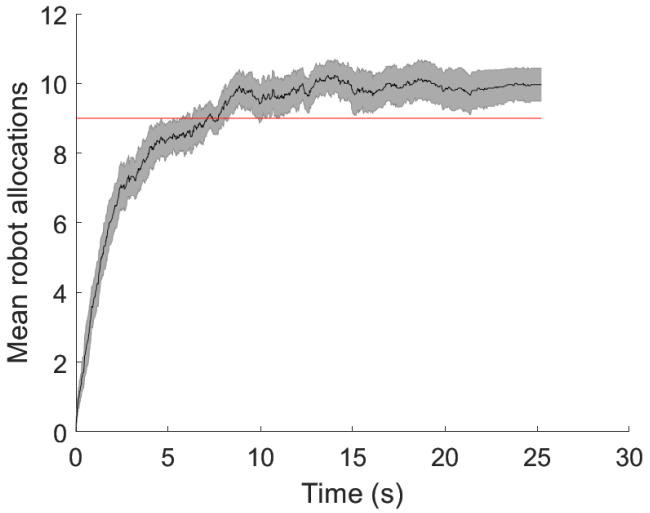

Figure A.1 Mean Robot Allocations over Time. Red line shows the target robot allocation around the payload

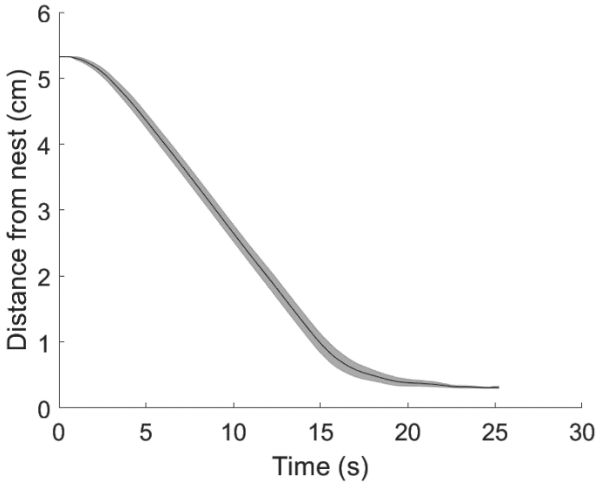

Figure A.2 Distance of Load from Destination over Time. Stopping distance was set to 0.3 cm

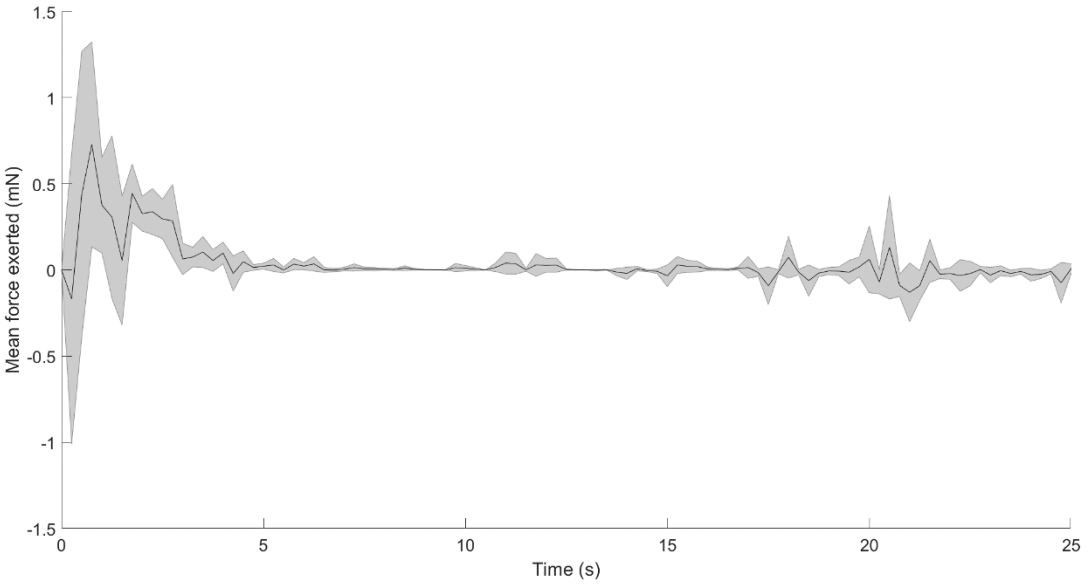

Figure A.3 Mean Value of Force Magnitude Exerted by Each Robot on the Payload. Values are sampled at 0.25 second intervals.

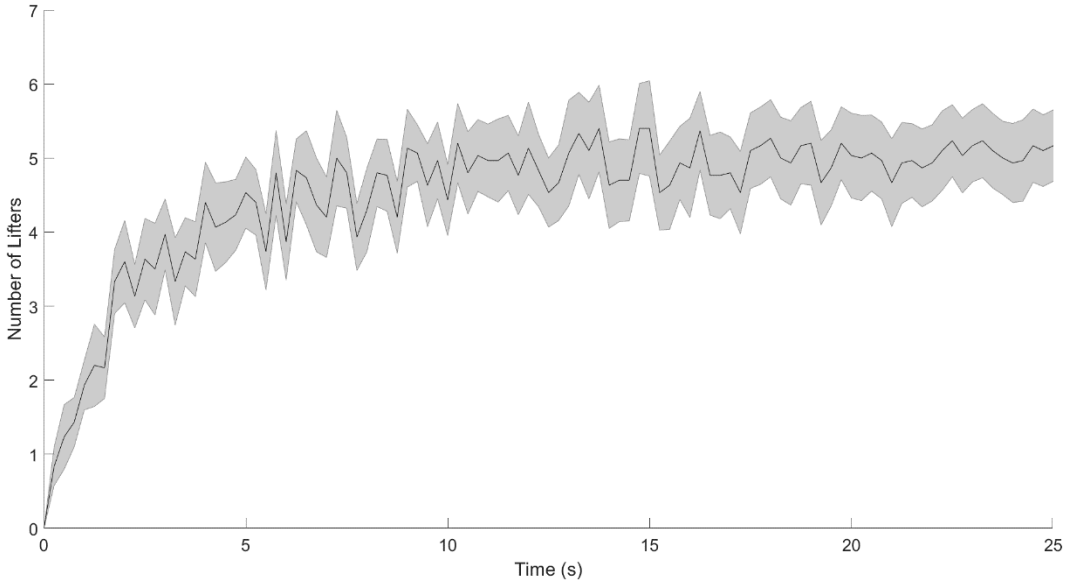

Figure A.4 Time Evolution of Number of Robots in Lifting Role, Sampled over Time Intervals of 0.25 seconds.

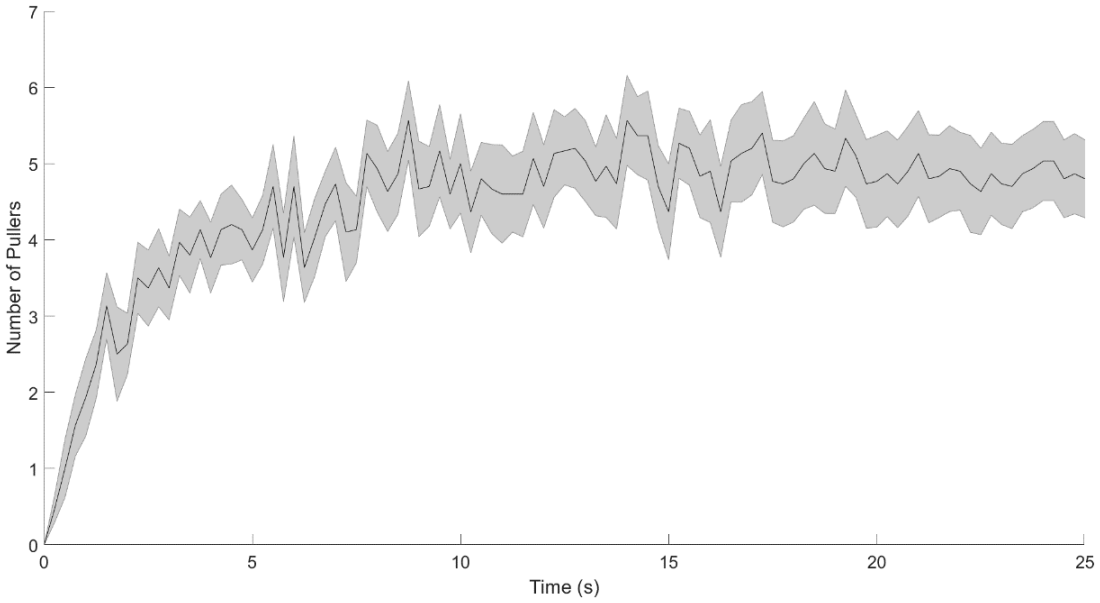

Figure A.5 Time Evolution of Number of Robots in Pulling Role, Sampled over Time Intervals of 0.25 seconds.

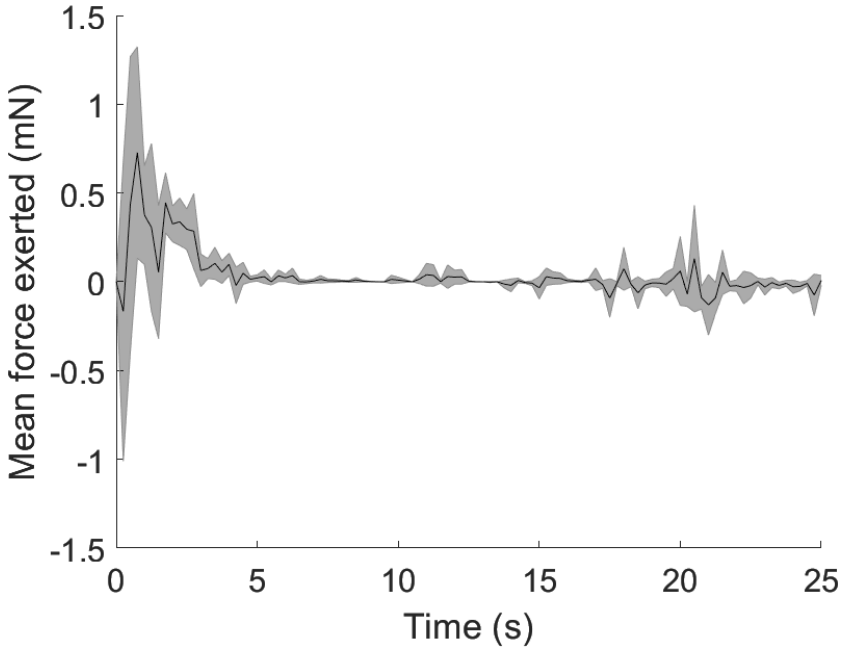

Figure A.6 Speed of Payload over Time under Action of Forces Exerted by the Attached Robots. Red line shows desired load velocity, 0.35 cm/s.

Results of Experiment 3

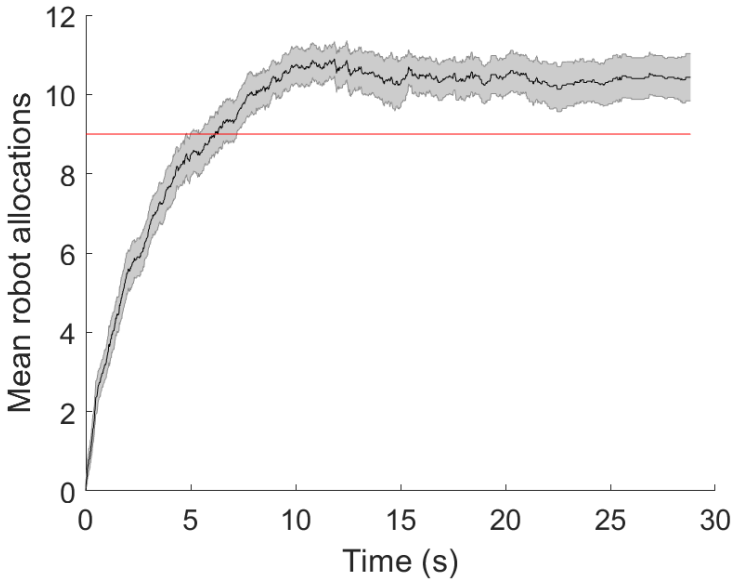

Figure A.7 Mean Robot Allocations over Time. Red line shows the target robot allocation around the payload

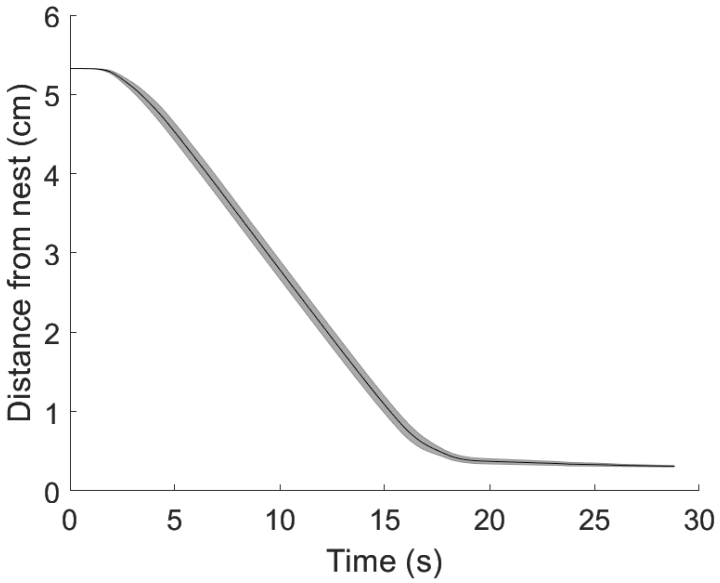

Figure A.8 Distance of Load from Destination over Time. Stopping distance was set to 0.3 cm

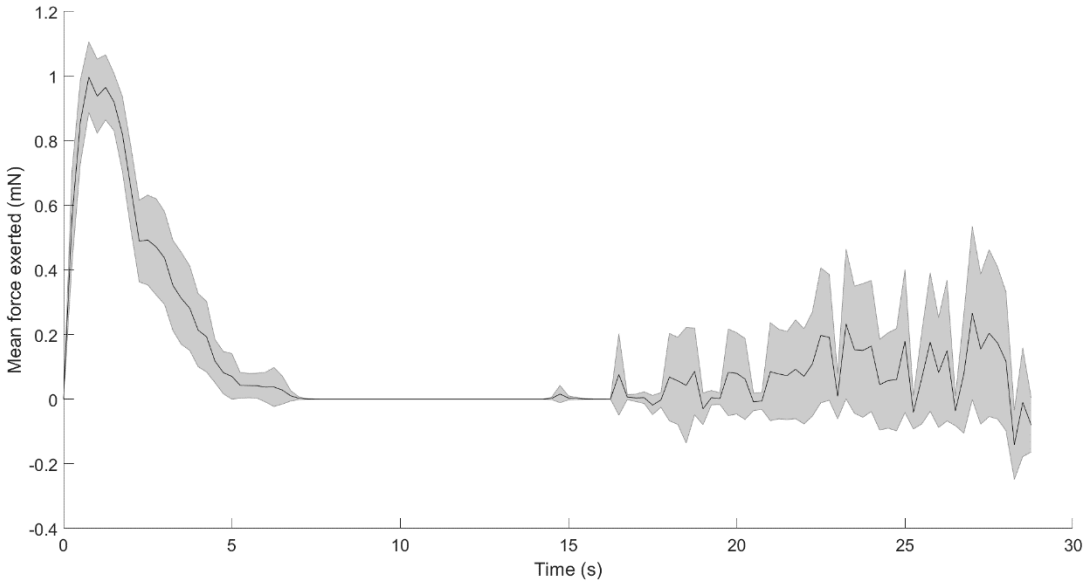

Figure A.9 Mean Value of Force Magnitude Exerted by Each Robot on the Payload. Values are sampled at 0.25 second intervals.

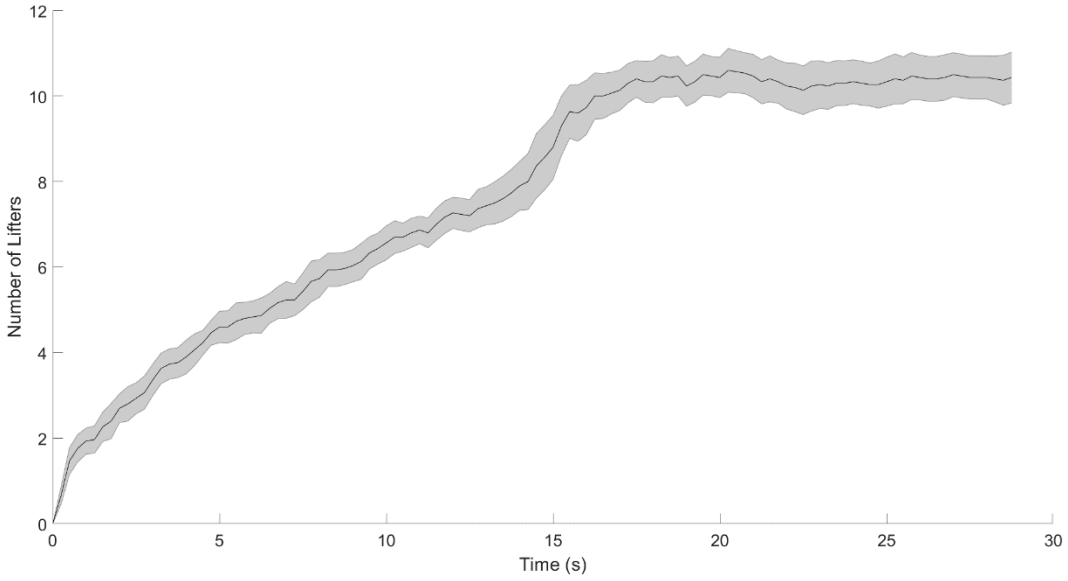

Figure A.10 Time Evolution of Number of Robots in Lifting Role, Sampled over Time Intervals of 0.25 seconds.

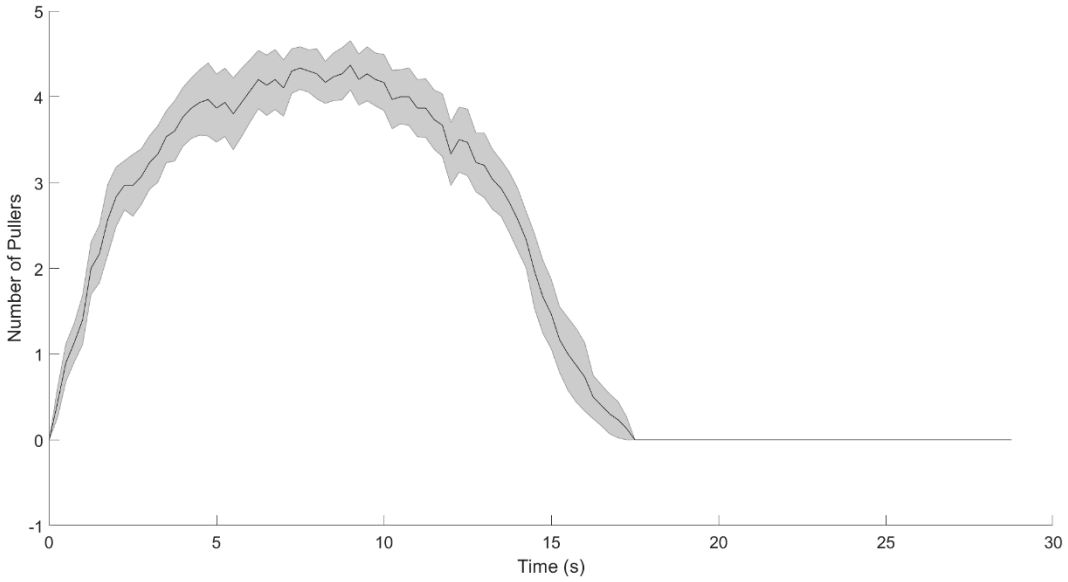

Figure A.11 Time Evolution of Number of Robots in Pulling Role, Sampled over Time Intervals of 0.25 seconds.

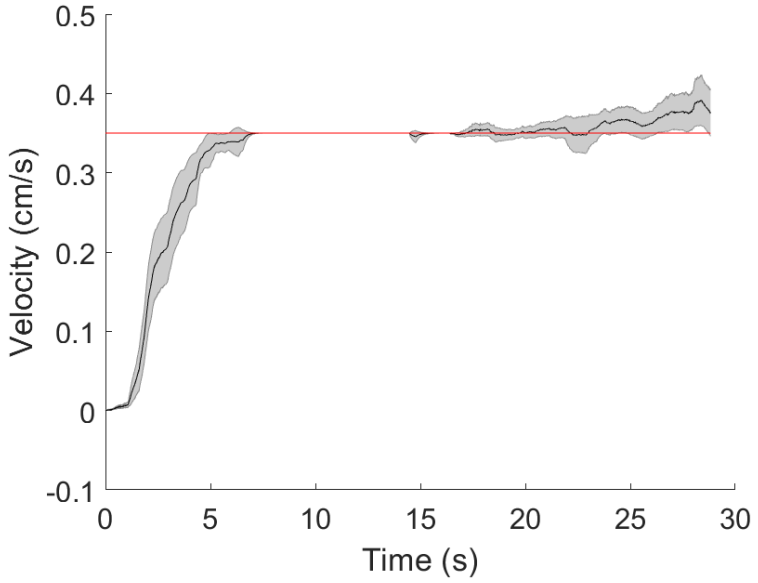

Figure A.12 Speed of Payload over Time under Action of Forces Exerted by the Attached Robots. Red line shows desired load velocity, 0.35 cm/s.

Results of Experiment 4

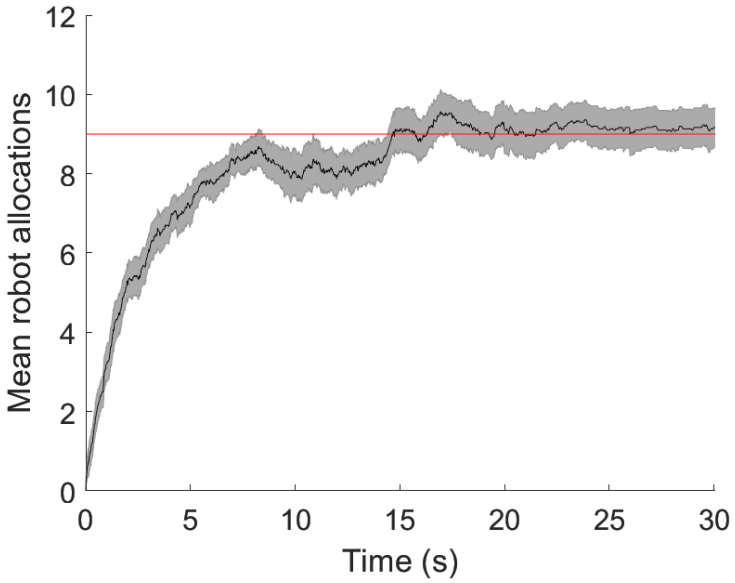

Figure A.13 Mean Robot Allocations over Time. Red line shows the target robot allocation around the payload

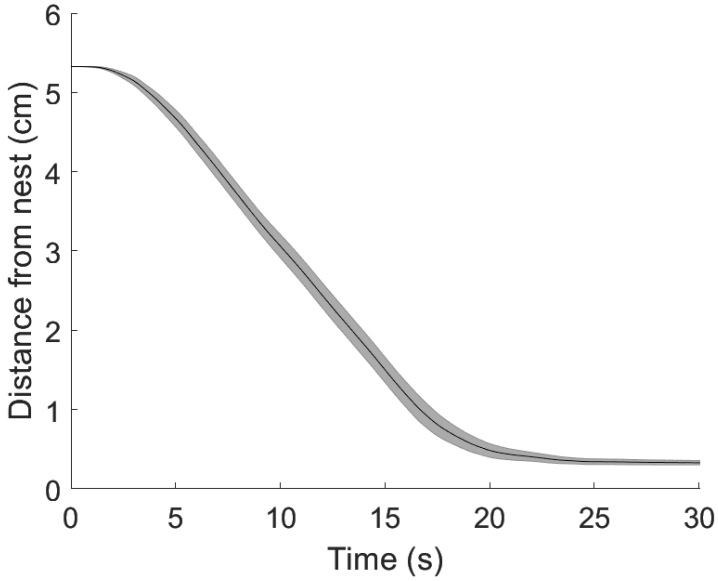

Figure A.14 Distance of Load from Destination over Time. Stopping distance was set to 0.3 cm

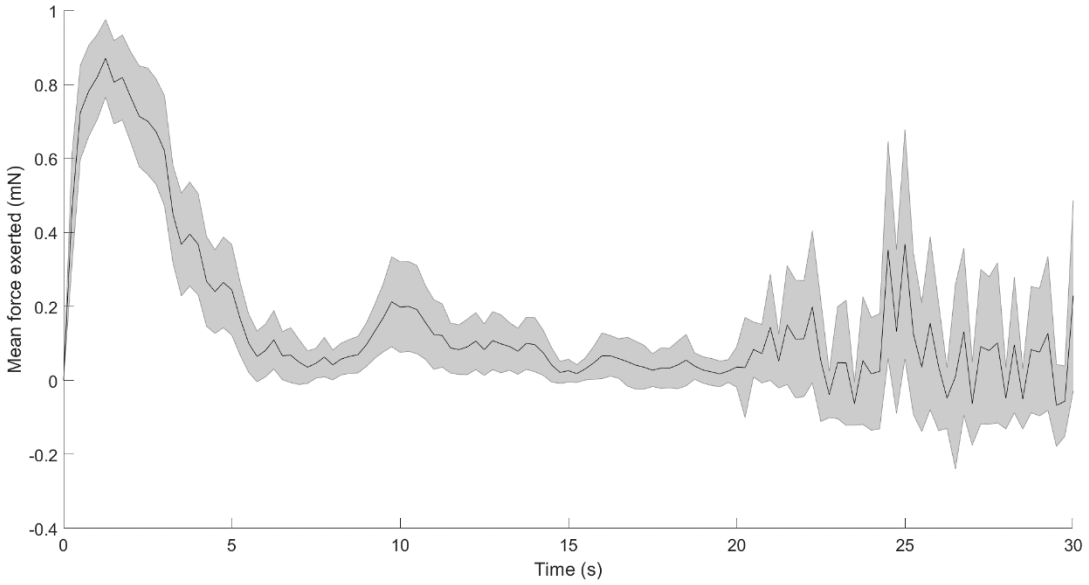

Figure A.15 Mean Value of Force Magnitude Exerted by Each Robot on the Payload. Values are sampled at 0.25 second intervals.

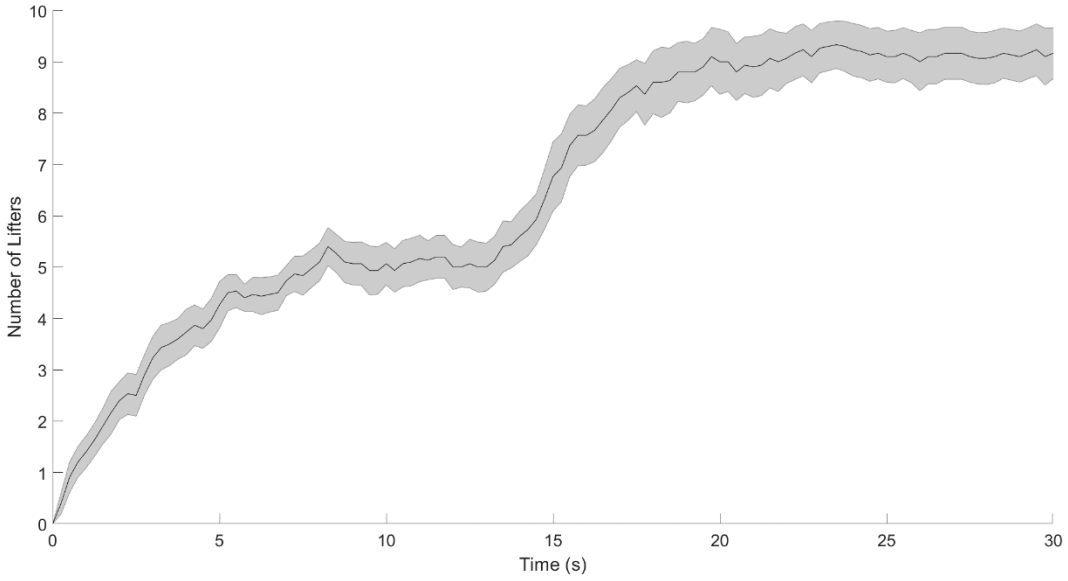

Figure A.16 Time Evolution of Number of Robots in Lifting Role, Sampled over Time Intervals of 0.25 seconds.

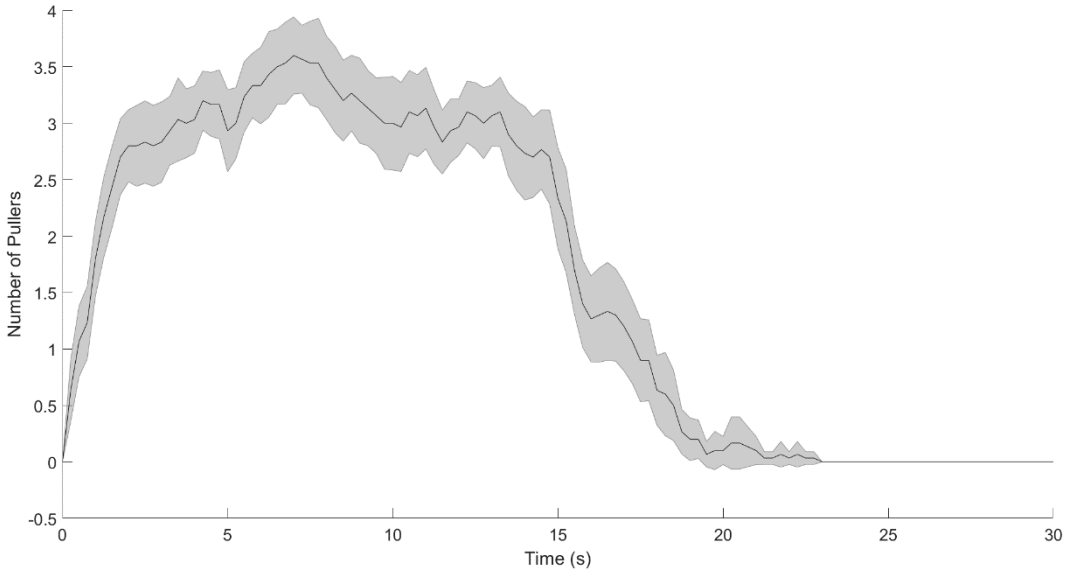

Figure A.17 Time Evolution of Number of Robots in Pulling Role, Sampled over Time Intervals of 0.25 seconds.

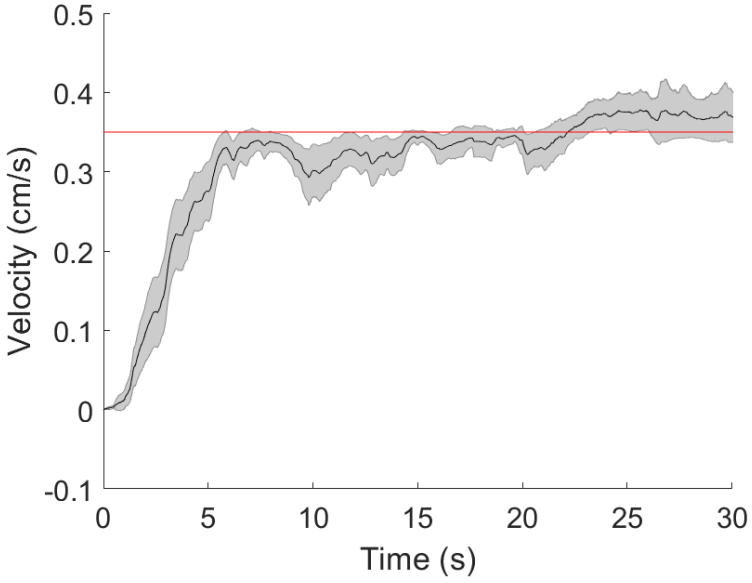

Figure A.18 Speed of Payload over Time under Action of Forces Exerted by the Attached Robots. Red line shows desired load velocity, 0.35 cm/s.

B. PLOTS OF EXPERIMENTAL RESULTS FOR SCENARIO 2

Experiment 2

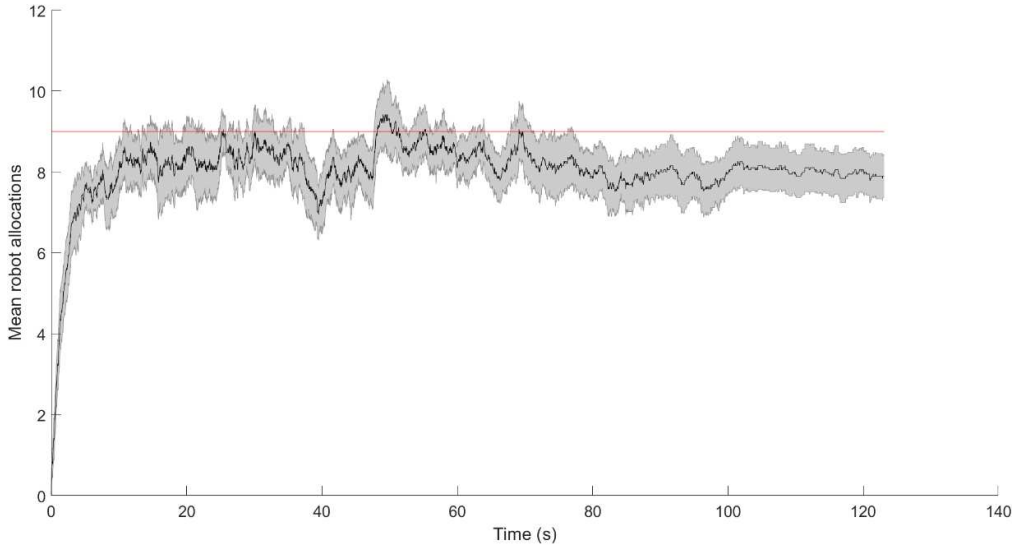

Figure B.1 Mean Robot Allocations over Time. Red line shows the target robot allocation around the payload (target ≈ 9).

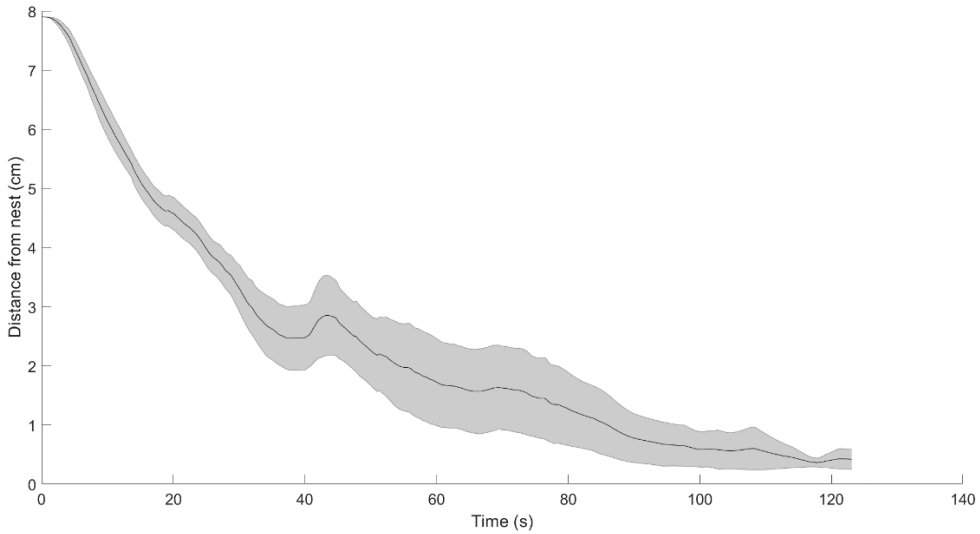

Figure B.2 Distance of Load from Destination over Time. Stopping distance was set to 0.3 cm

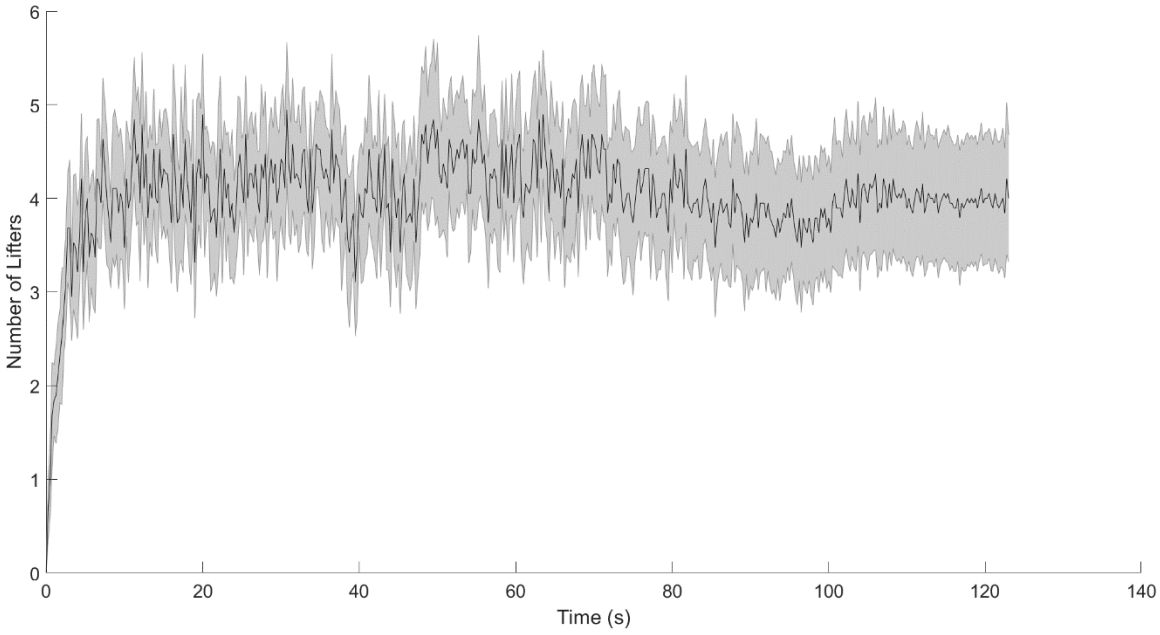

Figure B.3 Time Evolution of Number of Robots in Lifting Role, Sampled over Time Intervals of 0.25 seconds.

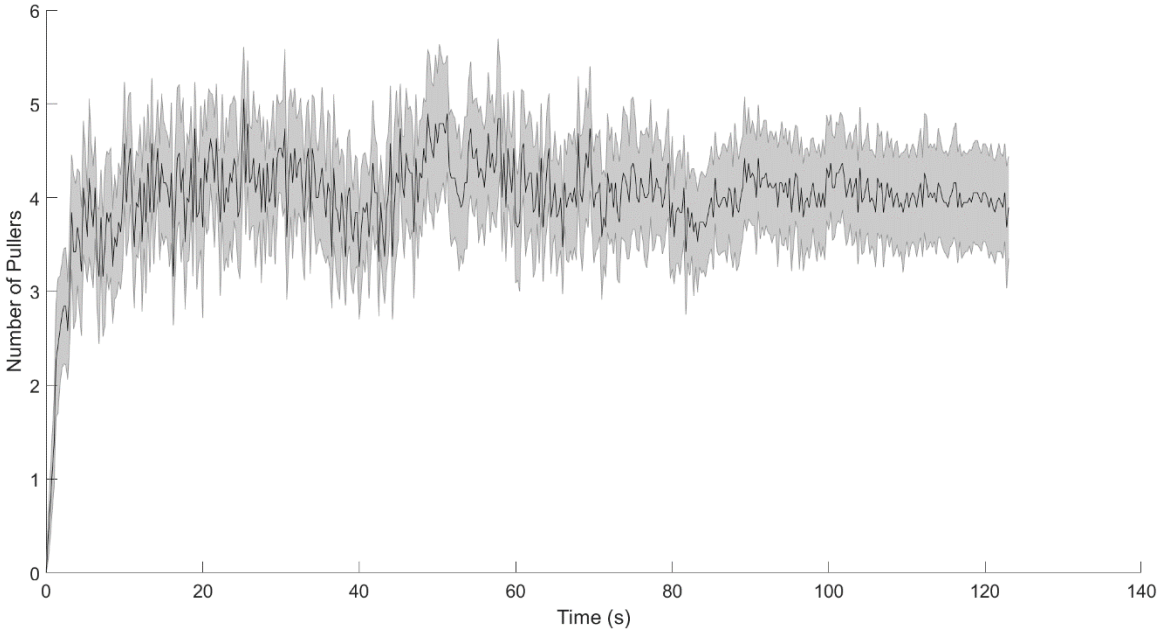

Figure B.4 Time Evolution of Number of Robots in Pulling Role, Sampled over Time Intervals of 0.25 seconds.

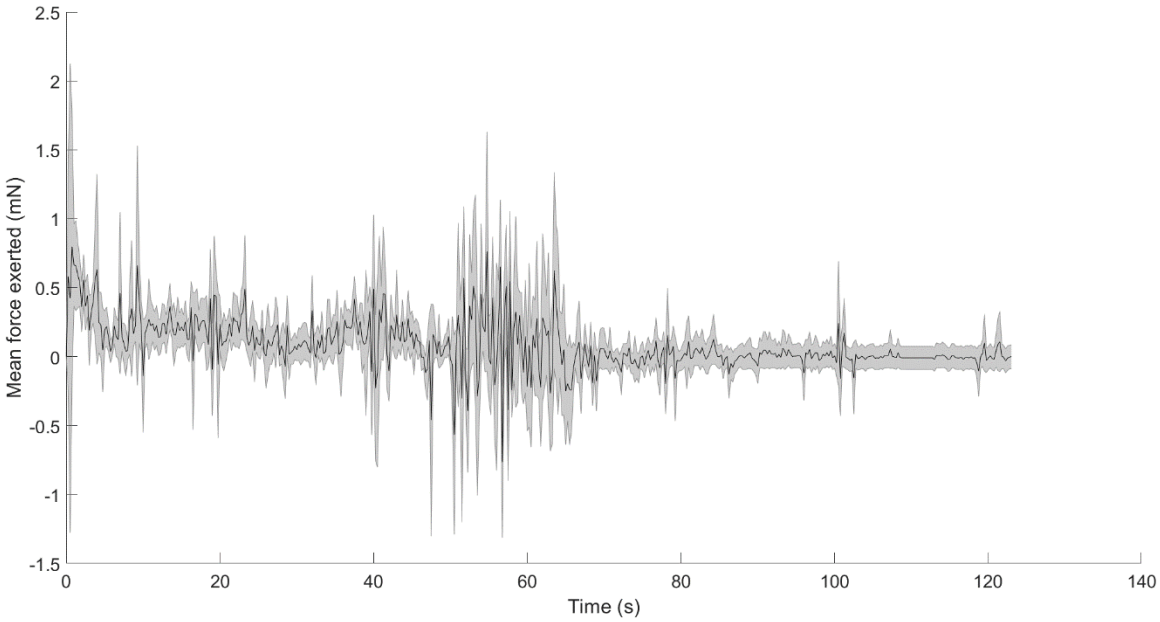

Figure B.5 Mean Value of Force Magnitude Exerted by Each Robot on the Payload. Values are sampled at 0.25 second intervals.

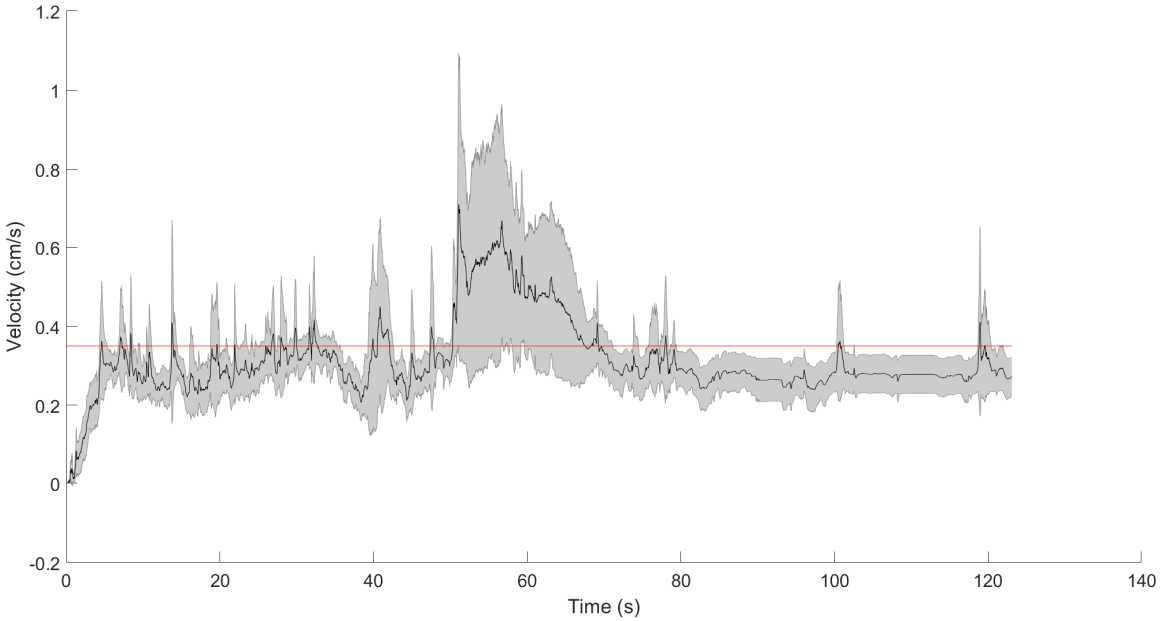

Figure B.6 Speed of Payload over Time under Action of Forces Exerted by the Attached Robots. Red line shows desired load velocity, 0.35 cm/s.

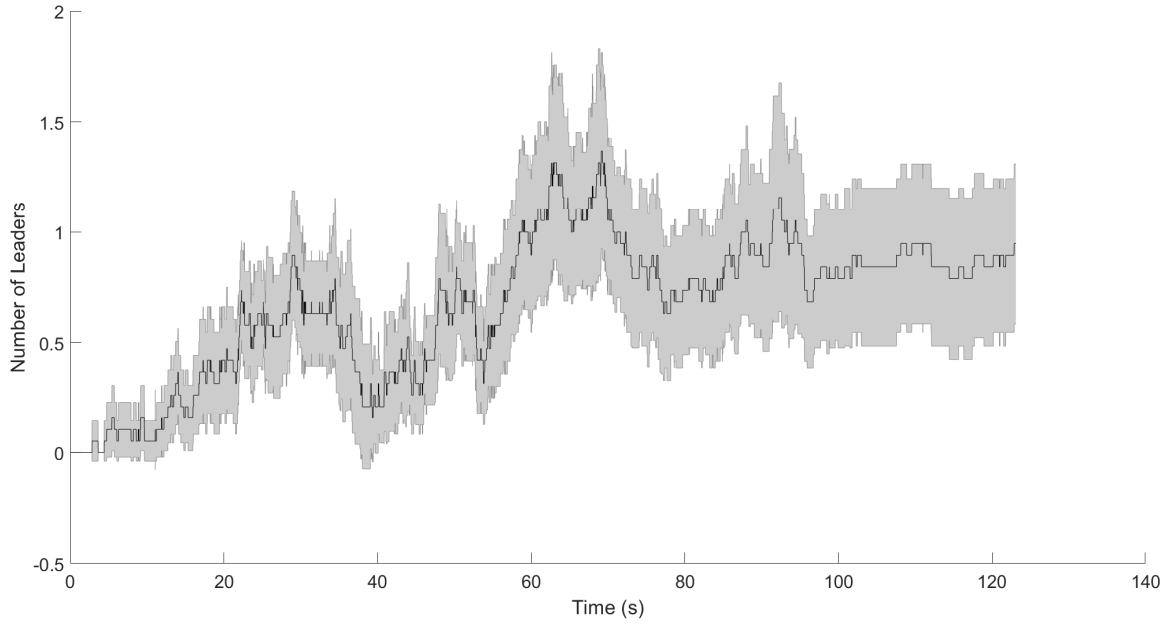

Figure B.7 Mean Number of Informed Robots Attached to Payload

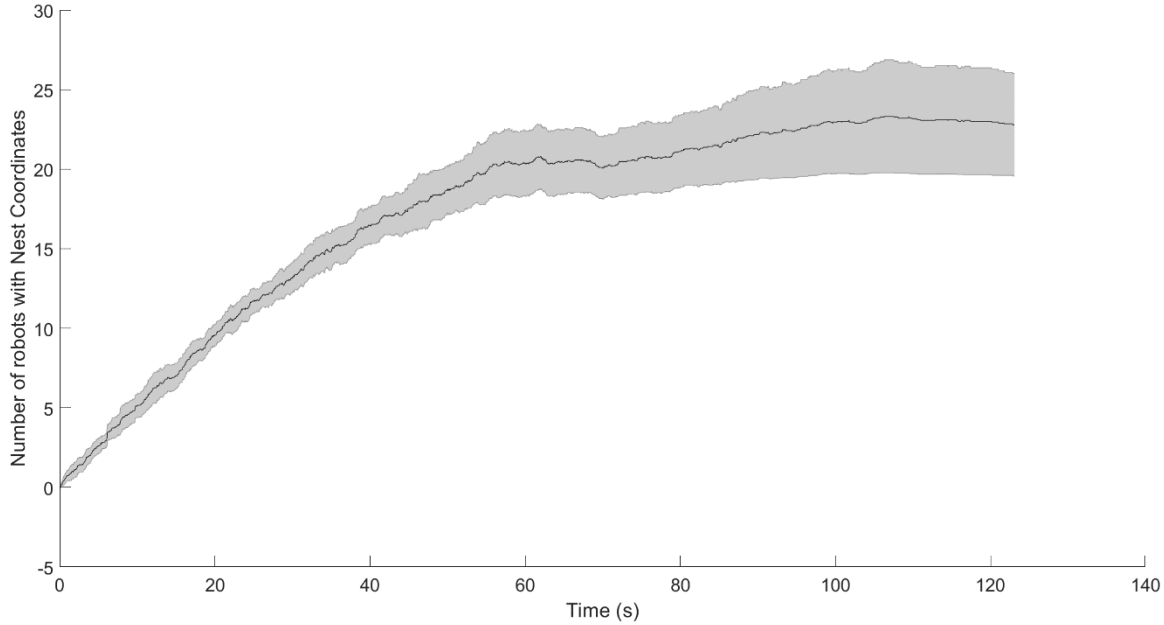

Figure B.8 Mean Number of Robots Informed with Nest Coordinates

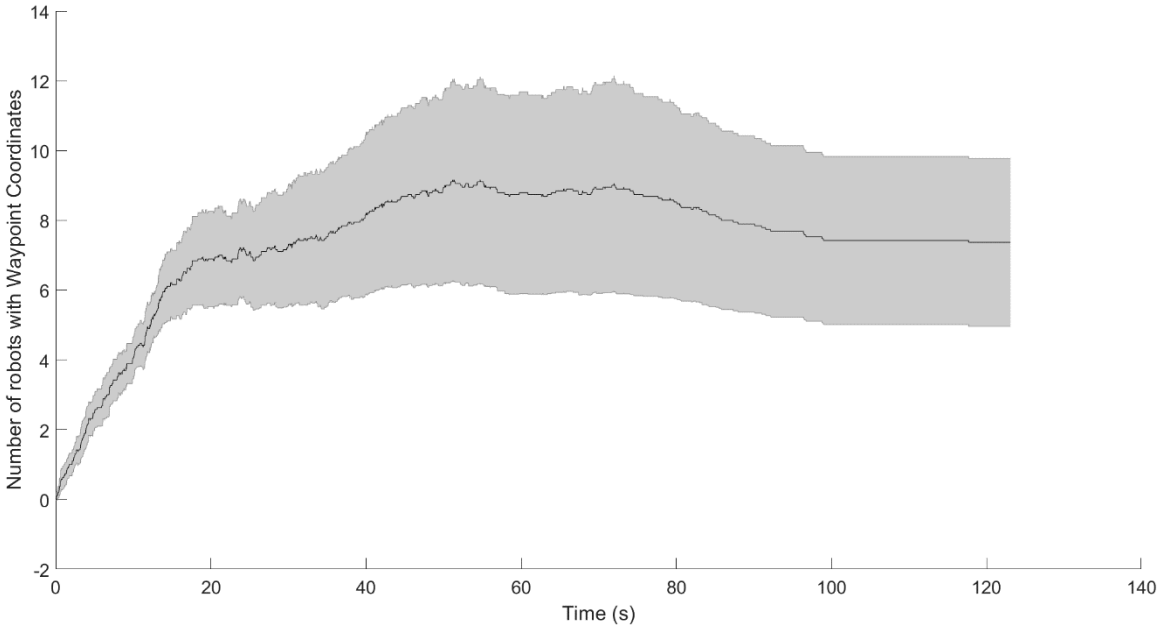

Figure B.9 Mean Number of Robots Informed with Waypoint Coordinates

Experiment 3

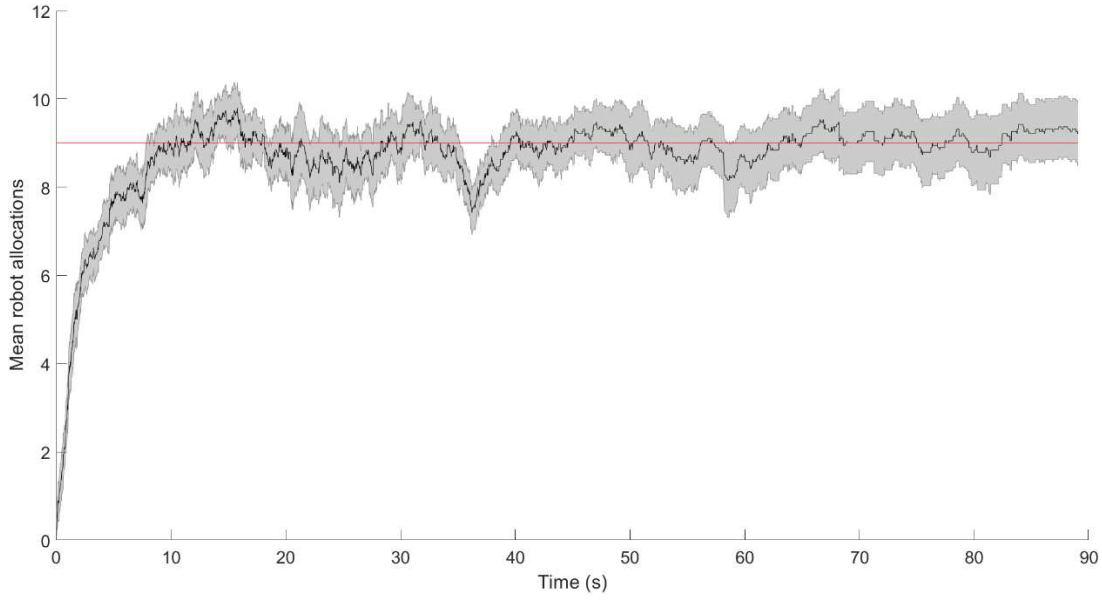

Figure B.10 Mean Robot Allocations over Time. Red line shows the target robot allocation around the payload (target ≈ 9).

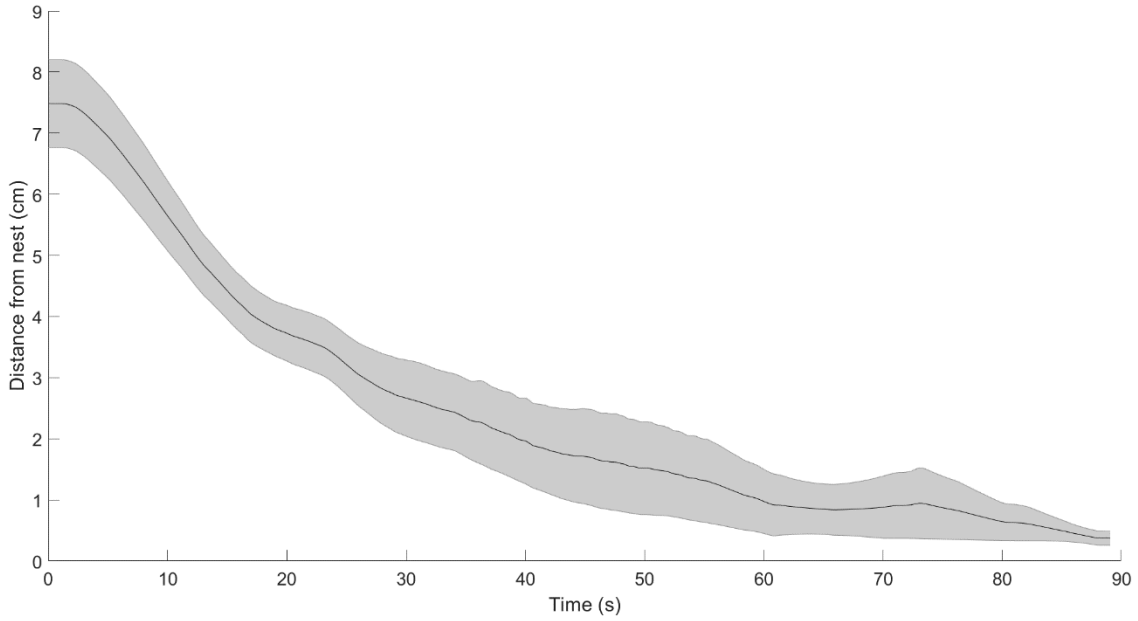

Figure B.11 Distance of Load from Destination over Time. Stopping distance was set to 0.3 cm

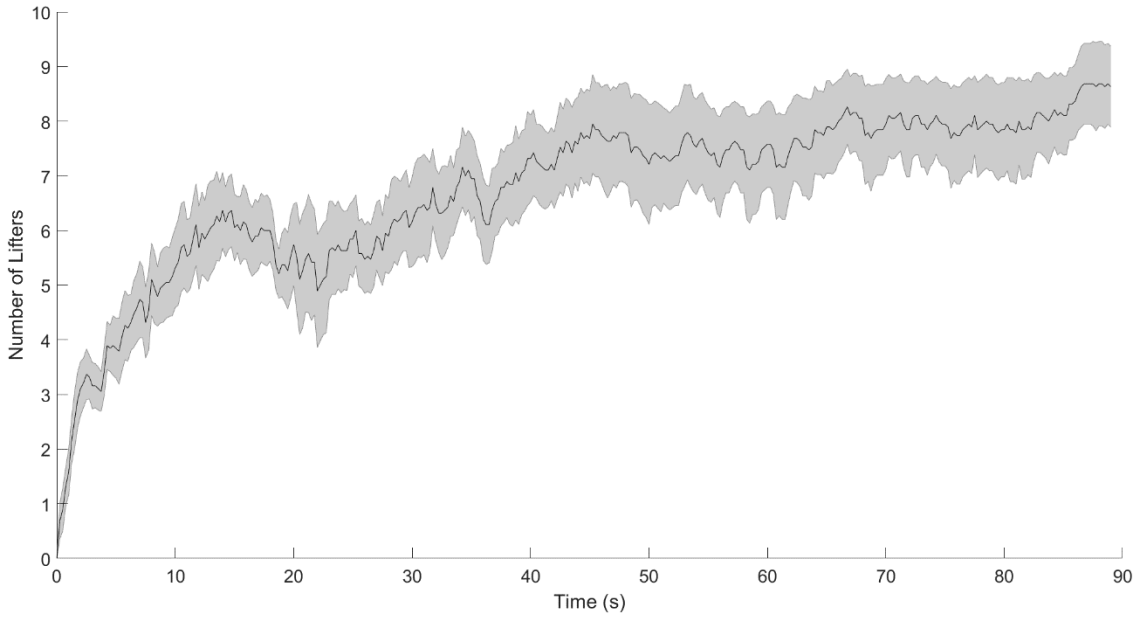

Figure B.12 Time Evolution of Number of Robots in Lifting Role, Sampled over Time Intervals of 0.25 seconds.

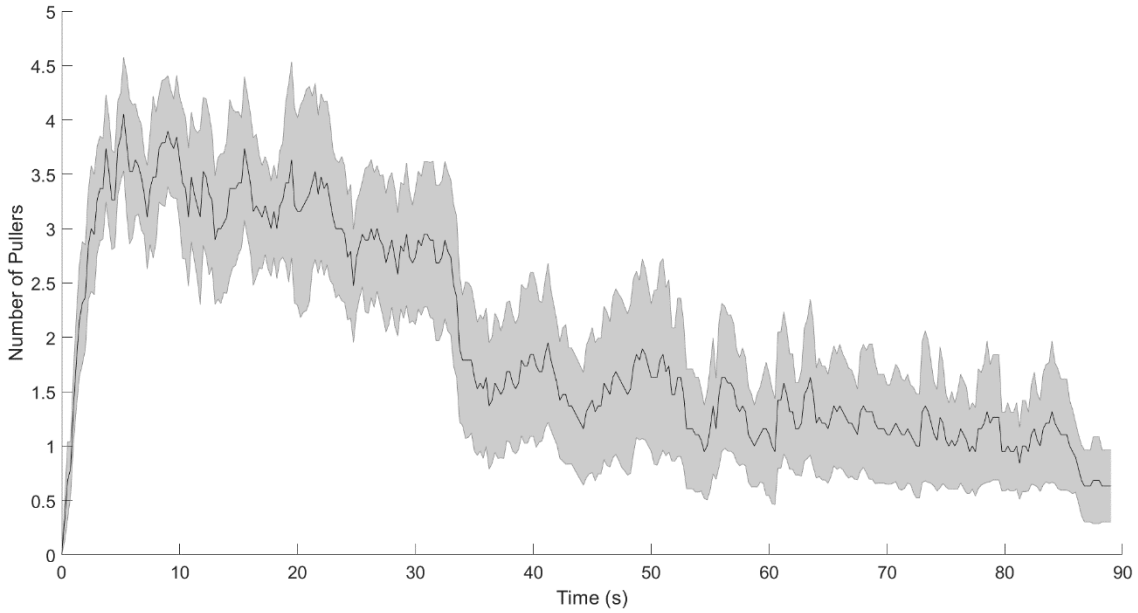

Figure B.13 Time Evolution of Number of Robots in Pulling Role, Sampled over Time Intervals of 0.25 seconds.

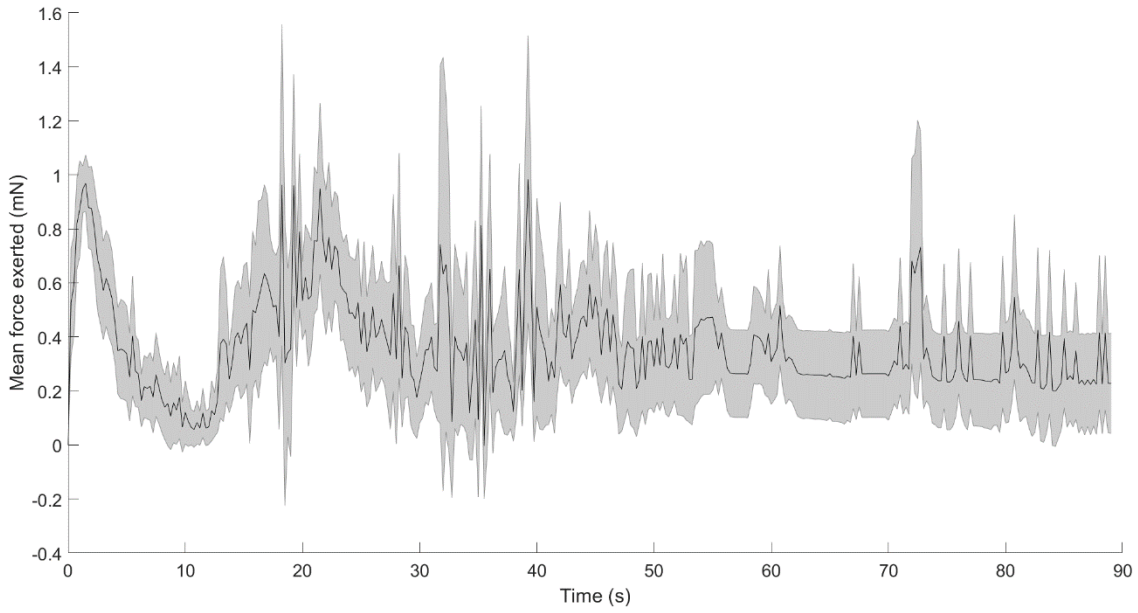

Figure B.14 Mean Value of Force Magnitude Exerted by Each Robot on the Payload. Values are sampled at 0.25 second intervals.

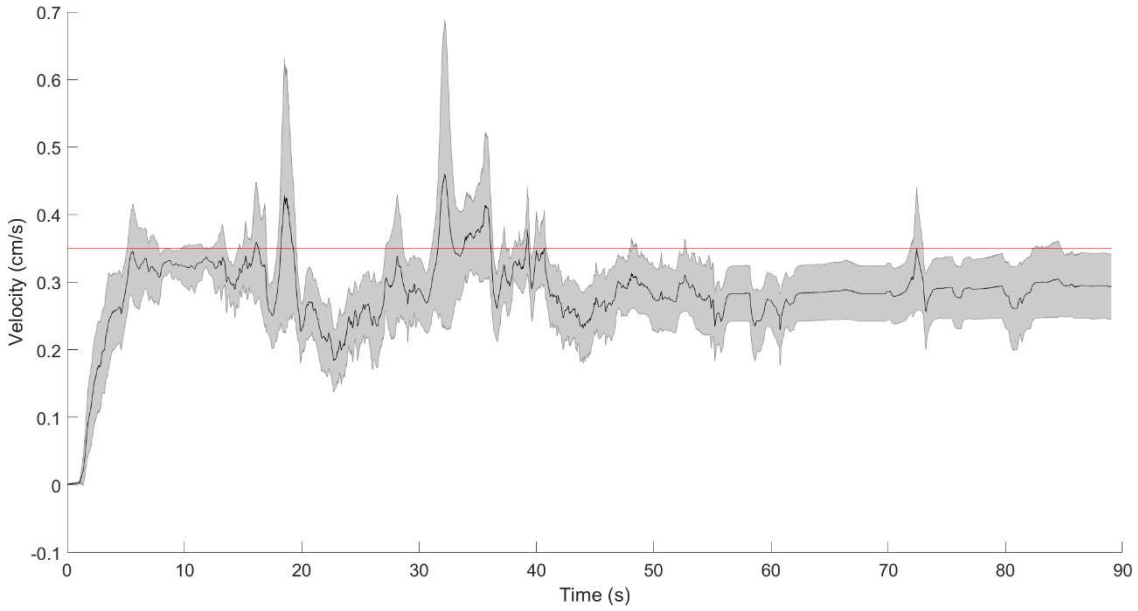

Figure B.15 Speed of payload over time under action of forces exerted by the attached robots.

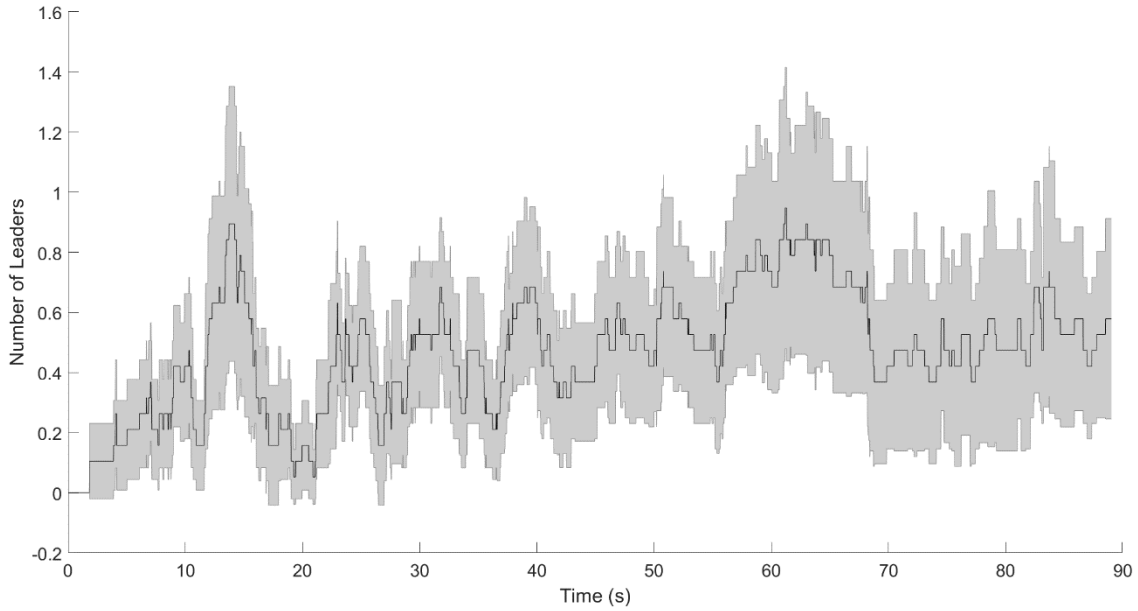

Figure B.16 Mean Number of Informed Robots Attached to Payload

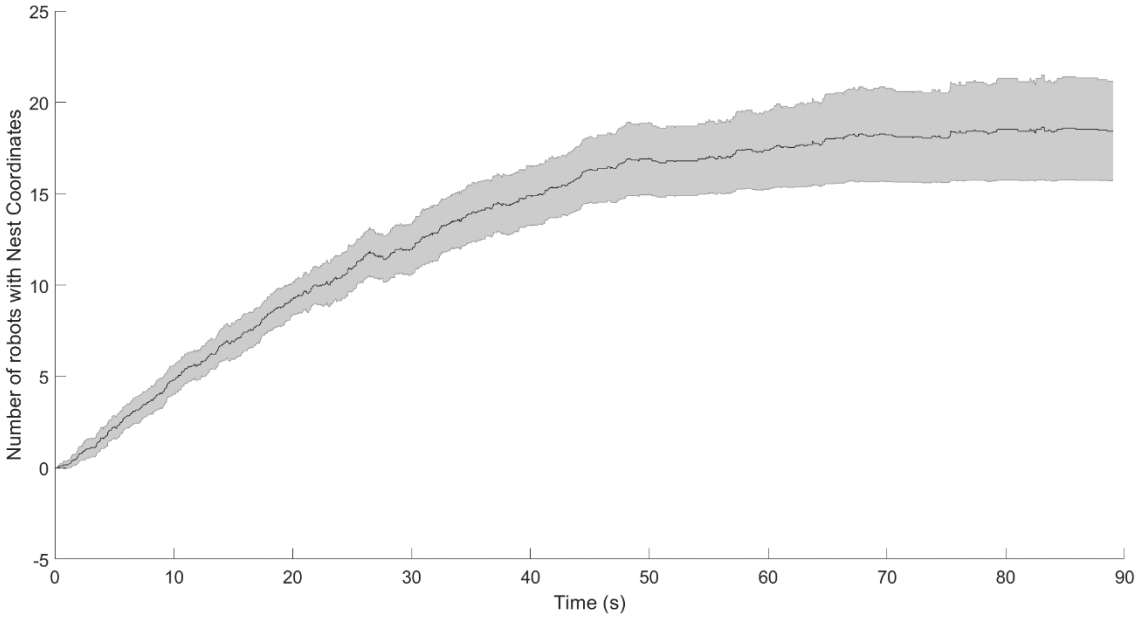

Figure B.17 Mean Number of Robots Informed with Nest Coordinates

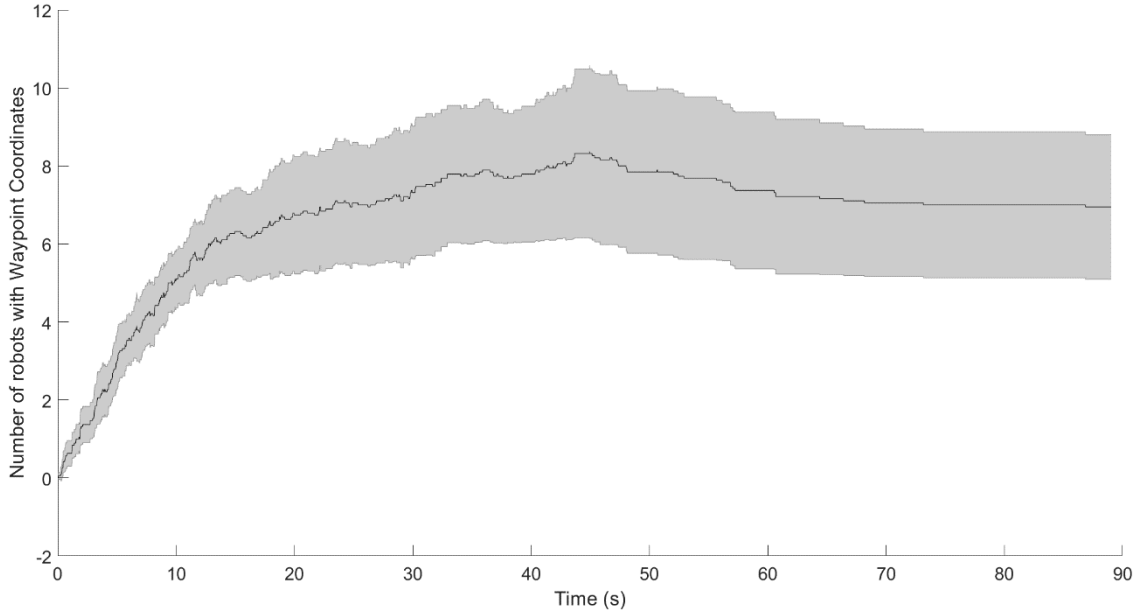

Figure B.18 Mean Number of Robots Informed with Waypoint Coordinates

Experiment 4

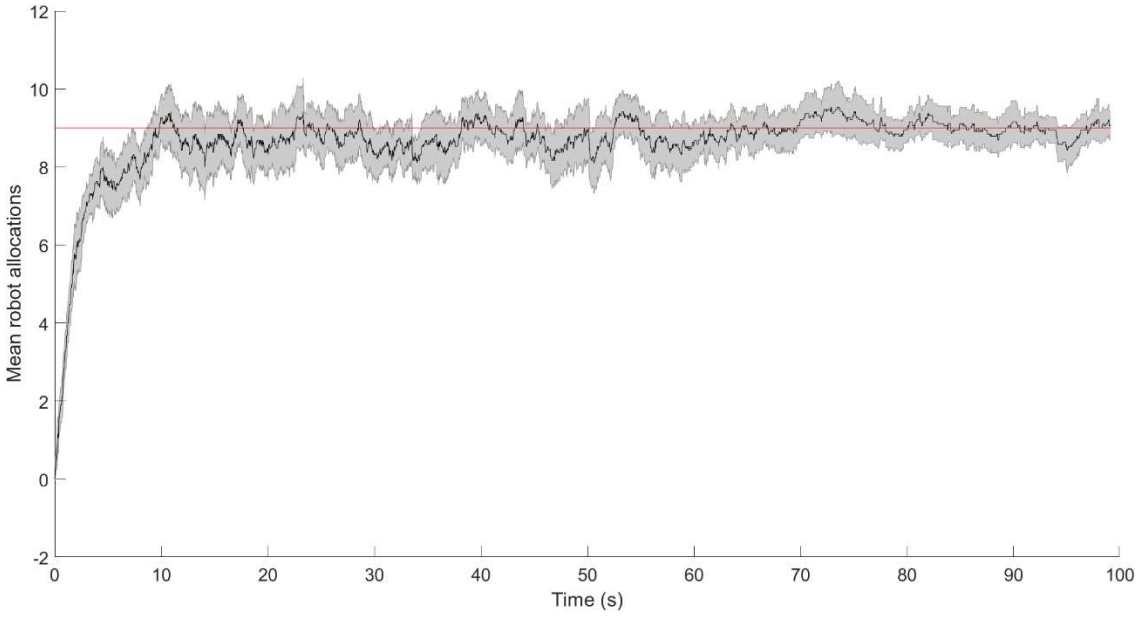

Figure B.19 Mean Robot Allocations over Time. Red line shows the target robot allocation around the payload (target ≈ 9).

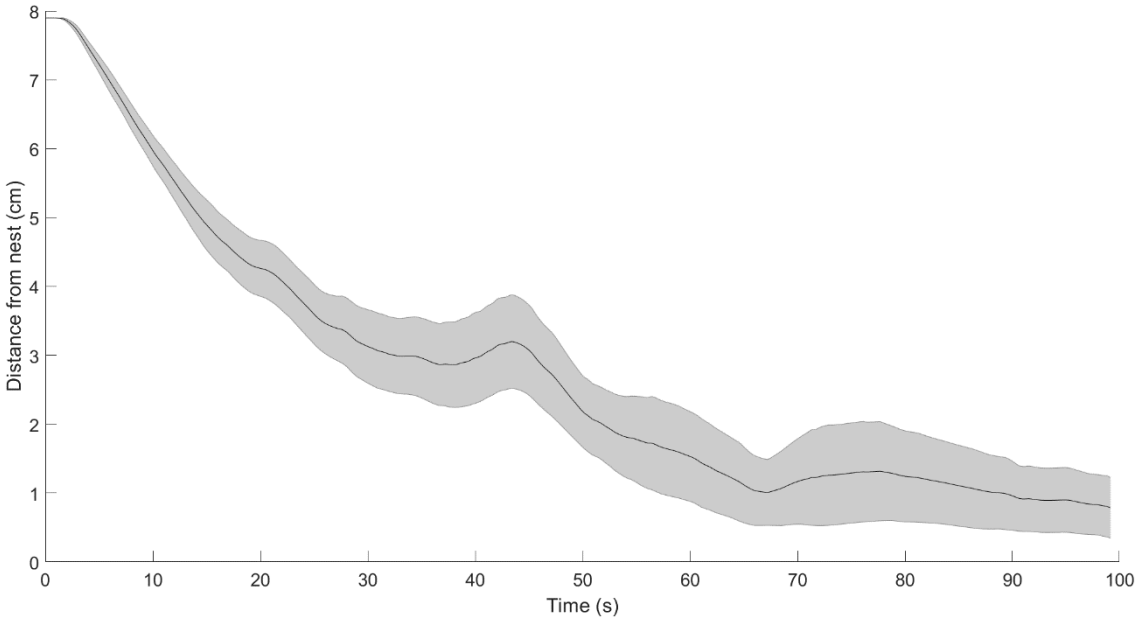

Figure B.20 Distance of Load from Destination over Time. Stopping distance was set to 0.3 cm

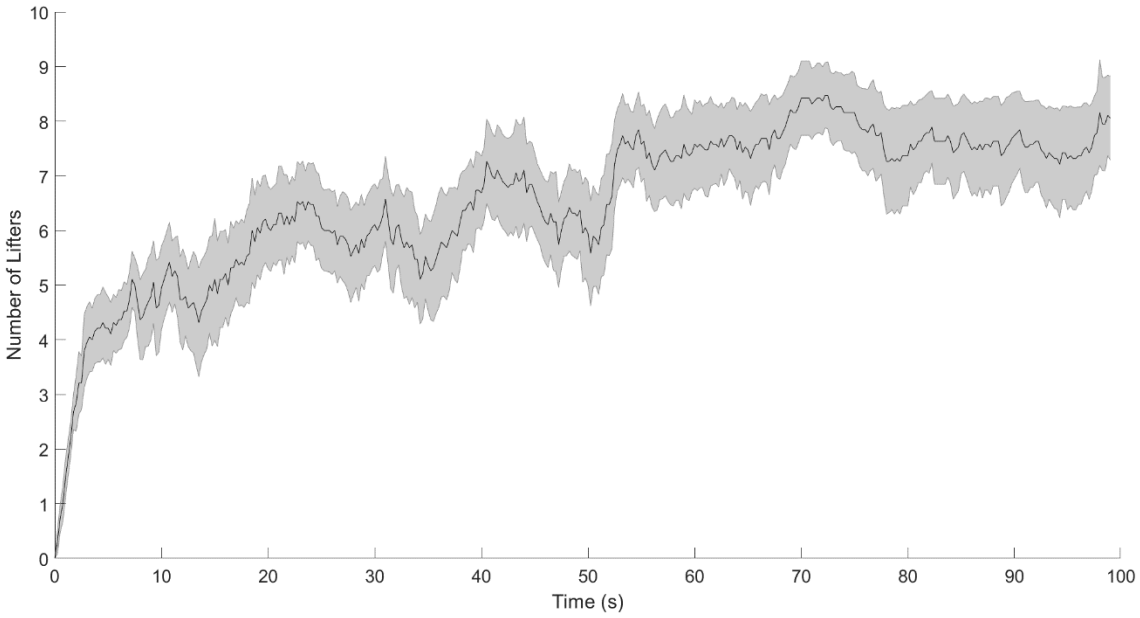

Figure B.21 Time Evolution of Number of Robots in Lifting Role, Sampled over Time Intervals of 0.25 seconds.

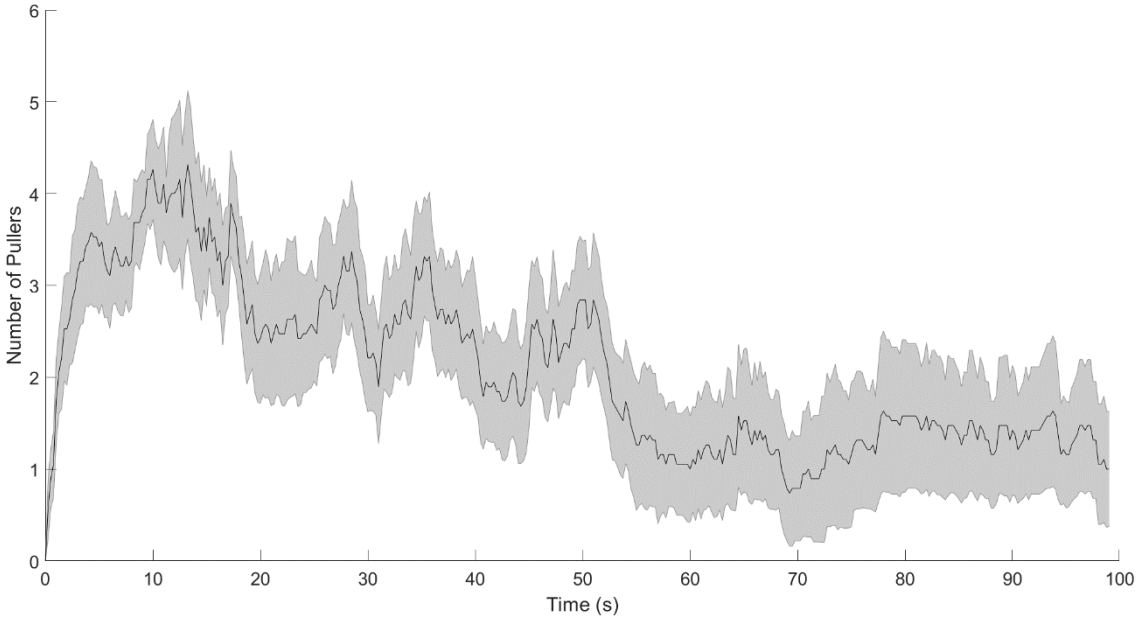

Figure B.22 Time Evolution of Number of Robots in Pulling Role, Sampled over Time Intervals of 0.25 seconds.

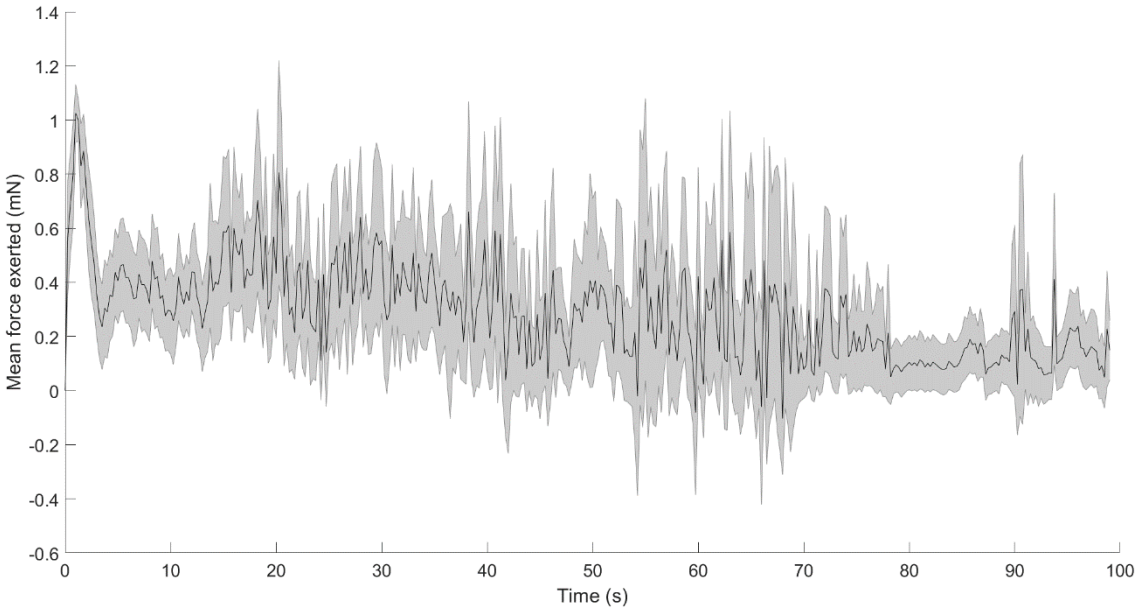

Figure B.23 Mean Value of Force Magnitude Exerted by Each Robot on the Payload. Values are sampled at 0.25 second intervals.

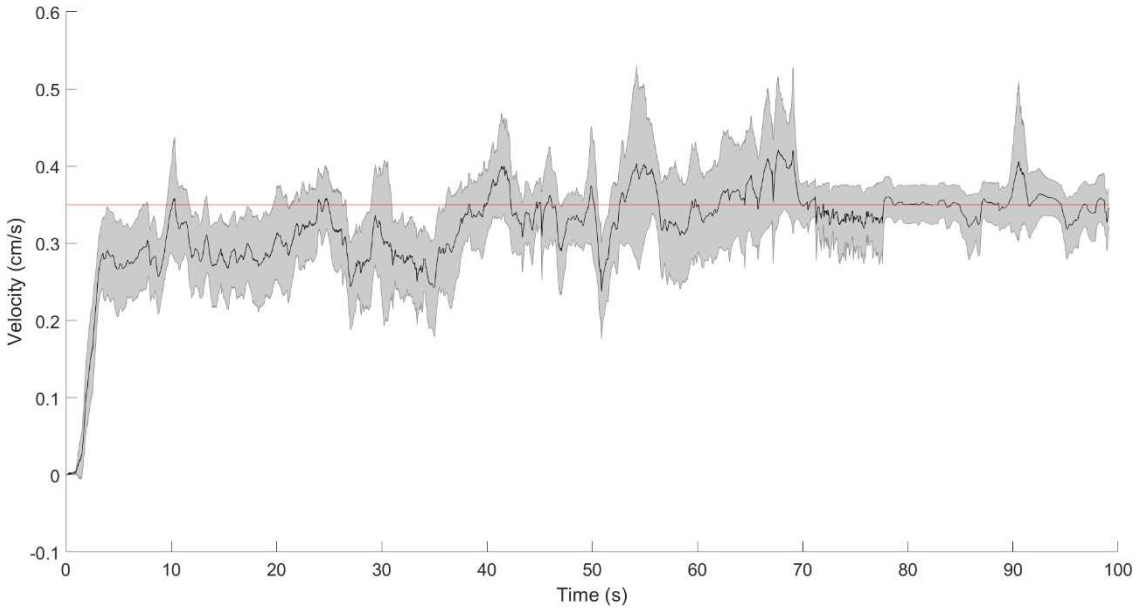

Figure B.24 Speed of payload over time under action of forces exerted by the attached robots.

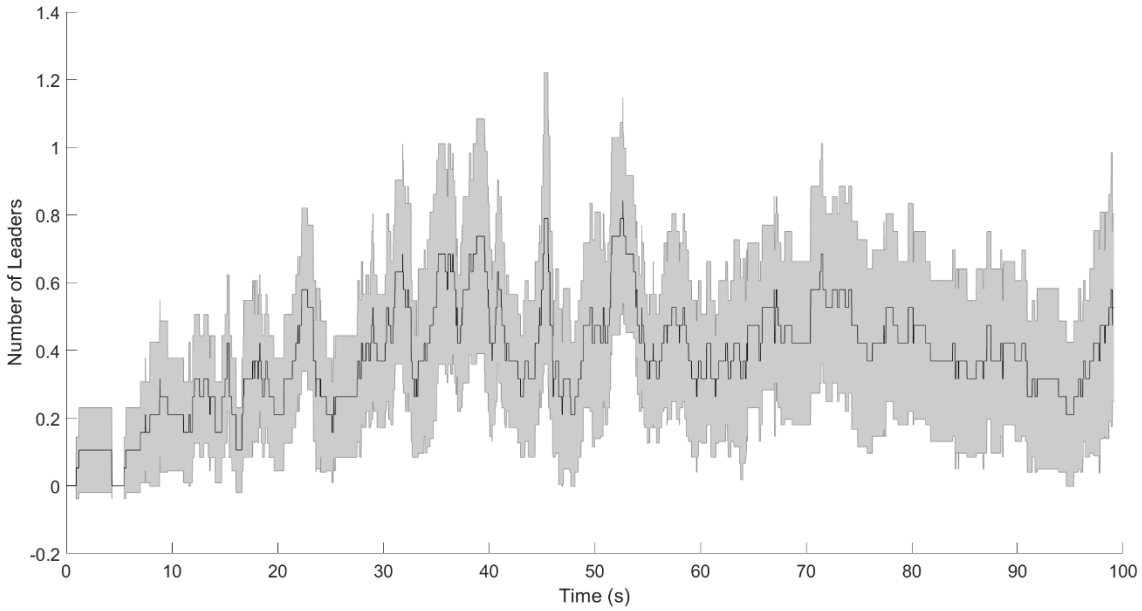

Figure B.25 Mean Number of Informed Robots Attached to Payload

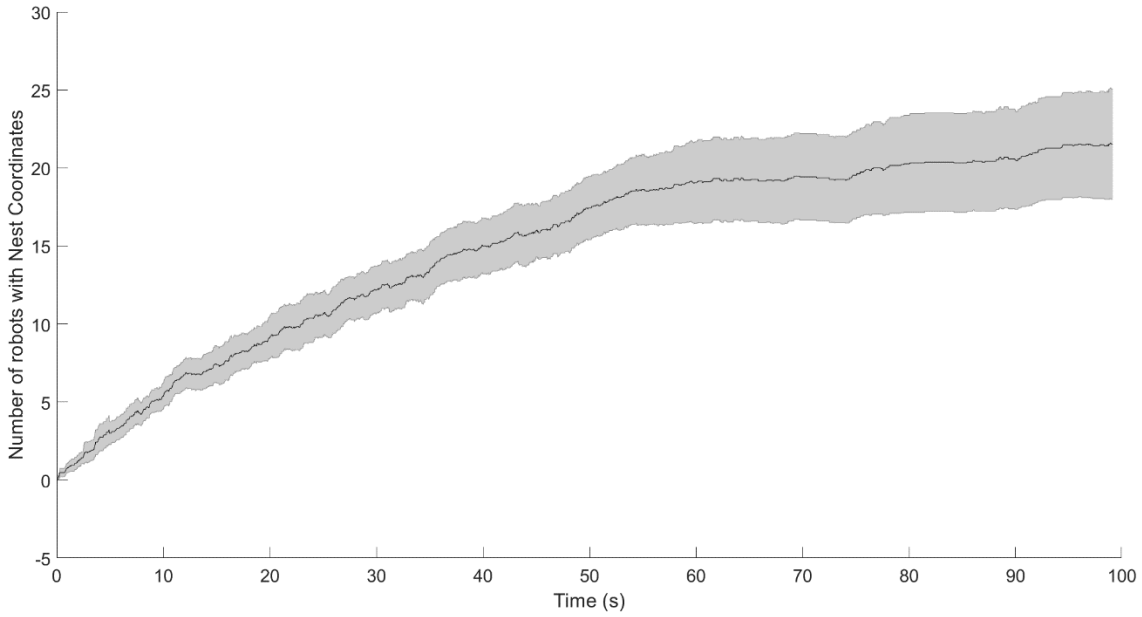

Figure B.26 Mean Number of Robots Informed with Nest Coordinates

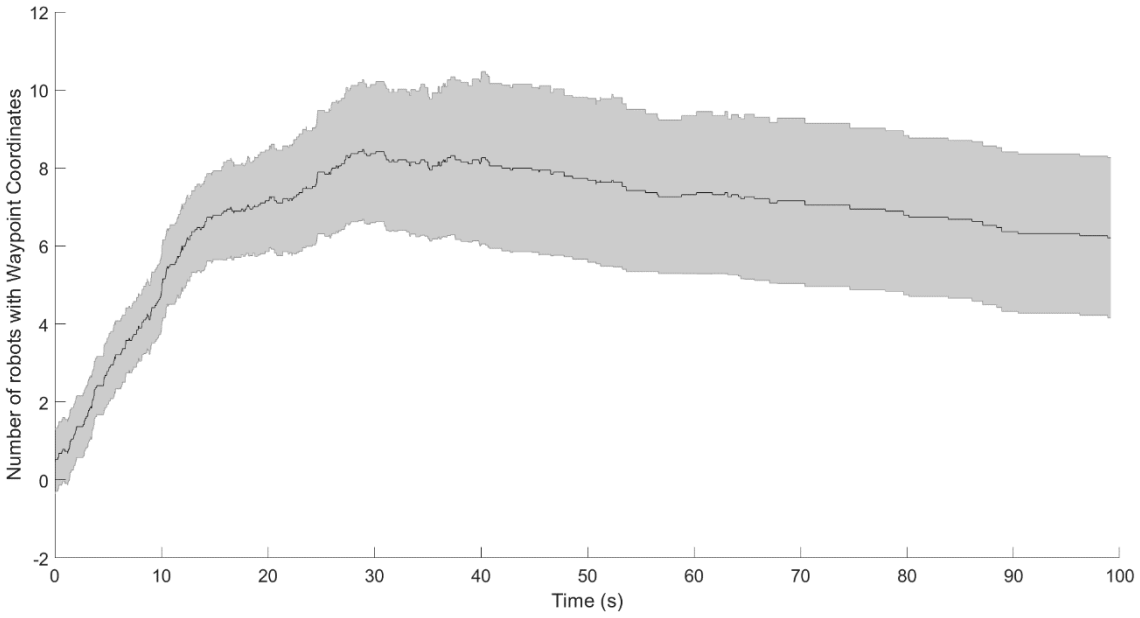

Figure B.27 Mean Number of Robots Informed with Waypoint Coordinates